Mon. Not. R. Astron. Soc. **392,** 718–732 (2009) doi:10.1111/j.1365-2966.2008.14085.x

The population of early-type galaxies at $1 < z < 2$ – new clues on their formation and evolution

P. Saracco,⋆ M. Longhetti and S. Andreon
INAF – Osservatorio Astronomico di Brera, Via Brera 28, 20121 Milano, Italy

Accepted 2008 October 13. Received 2008 October 3; in original form 2008 August 18

ABSTRACT

We present the morphological analysis based on *Hubble Space Telescope HST*-NICMOS (Near-Infrared Camera and Multi-Object Spectrometer) observations in the F160W filter ($\lambda \simeq 1.6\,\mu$m) of a sample of 32 early-type galaxies (ETGs) at $1 < z < 2$ with spectroscopic confirmation of their redshift and spectral type. The 32 ETGs at $\langle z \rangle \sim 1.5$ are placed on the $(\langle \mu \rangle_e, R_e)$ plane according to the Kormendy relation (KR) with the same slope of the local one but with a different zero-point, which accounts for the evolution they undergo from $z \sim 1.5$–2 to $z = 0$. The best fitting of their spectral energy distribution shows that ETGs at $1 < z < 2$ are composed of two distinct populations, an older population (oETGs) and a younger population (yETGs) whose mean ages differ by about 1.5–2 Gyr. Young ETGs are not denser than local ones since they follow the size–mass relation of local ETGs, and luminosity evolution brings them on to the local KR and size–luminosity relations without the need of size evolution. Old ETGs do not follow the size–mass relation of local ETGs, and luminosity evolution does not account for the discrepancy they show with respect to the local size–luminosity relation and KR. An increase in their R_e by a factor of 2.5–3 (a density decrease by a factor of 15–30) from $z \sim 1.5$–2 to $z \sim 0$ is required to bring these galaxies on to the local scaling relations. The different properties and the different behaviour shown by the two populations with respect to the scaling relations imply different formation and evolution scenarios. The older population of ETGs must have formed at a higher z in a sort of dissipative gas-rich collapse able to produce remnants which at $z \sim 2$ are old and compact, a scenario which can be fitted qualitatively by some recent hydrodynamic simulations of gas-rich mergers. Given the typical time-scale of merging and the old age of their stellar population, oETGs should exist as they are up to $z \gtrsim 3$–3.5. The size evolution they must experience from $z \sim 2$ to $\sim$0 must leave unchanged their mass to not exceed the local number of high-mass ($\mathcal{M}_* > 5 \times 10^{11}\,\mathrm{M}_\odot$) ETGs. Thus, major merging cannot fit this requirement. Satellite merging, close encounters and interactions can help at least qualitatively in solving this problem. The younger population of ETGs can be formed later through subsequent episodes of merging which increased progressively their size and assembled their mass down to $z \sim 2$. At $z < 2$, they evolve purely in luminosity since episodes of major merging would bring them far from the local scaling relations.

Key words: galaxies: elliptical and lenticular, cD – galaxies: evolution – galaxies: formation.

1 INTRODUCTION

The formation and the evolution of early-type galaxies (ETGs; elliptical and bulge-dominated galaxies) occupy an important position among the challenges of the observational cosmology. At least $\sim$70 per cent of the stellar mass in the local universe is locked into ETGs. For this reason, the understanding of their buildup and growth is fundamental to trace the galaxy mass assembly in the Universe. Their homogeneous properties, e.g. colours and scaling relations, make them an excellent probe to investigate the history of the stellar mass assembly of galaxies over cosmic times (see e.g. Renzini 2006 and references therein). Most of the recent studies based on samples of ETGs at $z < 1$ agree with considering completing their build up at $z \sim 0.8$. This statement is supported by the results on the evolution of the stellar mass function of galaxies which do not show any deficit of high-mass galaxies up to $z = 0.8$–1 (e.g. Fontana et al. 2004; Pozzetti et al. 2007), by the observed evolution of the bright end of the luminosity function of galaxies consistent with the pure luminosity evolution expected for early-types (e.g. Drory et al. 2005; Saracco et al. 2006; Zucca et al. 2006; Caputi et al. 2007; Cirasuolo et al. 2007, 2008), by the

⋆E-mail: paolo.saracco@brera.inaf.it

observed number density of ETGs at $z \leq 1$ consistent with the one at $z = 0$ (e.g. Saracco et al. 2005; Cimatti, Daddi & Renzini 2006; Conselice et al. 2007) and by the evolution of the size–mass (SM) and size–luminosity (SL) relations compatible with a passive luminosity evolution (e.g. McIntosh et al. 2005). If on one hand the agreement among these results provides a clear view of the status and of the evolution of ETGs at $z < 1$, they do not add stringent constraints on the mechanism(s) with which ETGs assemble their mass, pushing at higher z the redshift range of interest.

Several studies, indeed, suggest that both the observational and the theoretical efforts aimed at constraining the buildup of the stellar mass of ETGs and the shaping of their morphology should be focused at $1 < z < 2$, the redshift range for which the strongest evolution is expected (e.g. Glazebrook et al. 2004; Arnouts et al. 2007). The picture at this redshift is far from being as clear and homogeneous as at $z < 1$ because of the difficulties in catching ETGs at high redshift. Indeed, to study the population of ETGs at $1 < z < 2$, a preliminary but not so obvious step has to be overcome: the identification of suitable samples of ETGs with secure redshift determination, spectral classification and confirmed morphological signatures similar to those of the local ETGs. In fact, up to now, only few samples of spectroscopically identified ETGs at $z > 1$ have been collected, with no more than a tenth of galaxies morphologically confirming each: the sample of McCarthy et al. (2004) resulting from the Galaxy Deep–Deep Survey (GDDS) sample (Abraham et al. 2004) contains 10 galaxies at $z \sim 1.6$; the sample of Longhetti et al. (2005) derived from the TNG EROs Spectroscopic Identification Survey (TESIS) (Saracco et al. 2003) contains 10 galaxies at $z \sim 1.4$ and the sample of Cimatti et al. (2008) resulting from the K20 (Cimatti et al. 2002) and the Galaxy Mass Assembly Ultradeep Spectroscopic Survey (GMASS) surveys contains 13 galaxies at $z \sim 1.6$. On the basis of the analysis of these few samples, it is well ascertained that ETGs at $z \sim 1$–2 contain stellar populations formed in an intense and short-lived starburst at $z > 3$ (Cimatti et al. 2004; Longhetti et al. 2005; Farrah et al. 2006; Kong et al. 2006; McGrath et al. 2007). This information provides a strong constraint on the star formation history (SFH) of the stellar population of ETGs, that is the epoch at which the stars they host formed. On the other hand, this does not constrain how ETGs grew up: what are the time-scale and the mechanism(s) characterizing the growing and the shaping of ETGs?

Recently, evidence for higher compactness of the ETGs at $z > 1$ with respect to the local ones has come out. Daddi et al. (2005) show that a large fraction of their ETGs have smaller sizes (effective radii $R_e \sim 1$ kpc) than local ETGs of comparable stellar mass, possibly implying higher stellar densities even if the presence of active galactic nuclei in some of them could justify the compactness. However, other studies find similar results confirming the apparent smaller sizes of high-z ETGs if compared to the local ETGs with comparable stellar mass (e.g. Cassata et al. 2005; di Serego Alighieri et al. 2005; Trujillo et al. 2006a). These results are based on *Hubble Space Telescope* (*HST*) optical observations sampling the blue and ultraviolet (UV) rest-frame emission of the galaxies and/or on seeing-limited ground-based observations, characteristics which could affect the estimate of the effective radius of high-z ETGs. Moreover, the above results have been obtained by comparing galaxies at different redshift having, in principle, the same stellar mass. However, the stellar mass estimate depends on the spectrophotometric models used to fit the data and on the different model parameters. More recently, Longhetti et al. (2007) have studied the KR for a sample of ETGs at $z \sim 1.5$ using *HST*-NICMOS (Near-Infrared Camera and Multi-Object Spectrometer) observations. They show that these ETGs are at least two times more compact than those in the local Universe showing that this apparent high compactness is real and not dependent on the wavelength of observation (see also McGrath et al. 2008 and Buitrago et al. 2008 for similar recent results). Some of these works are based on the small samples quoted above made of a tenth of galaxies spanning a narrow range in luminosity and stellar mass or on samples of candidates ETGs with no confirmation of their redshift and spectral type.

In an attempt to provide new and stronger constraints on the formation of compact/denserhigh-z ETGs, we have studied the main scaling relations [the Kormendy relation (KR), the SL and the SM relations] for a new sample of 32 ETGs at $1 < z < 2$ with spectroscopic confirmation of their redshift and spectral type. The morphological analysis for the whole sample is based on *HST*-NICMOS imaging in the F160W filter ($\lambda \sim 1.6\,\mu$m) which samples the rest-frame *R* band at the redshift of the galaxies. The sample spans 3 mag in absolute magnitude and more than two orders of magnitude in stellar mass. This paper presents the analysis and the results we obtained from the study of the scaling relations and is organized as follows. Section 2 is a presentation of our sample describing the criteria used to construct the sample and the data we have at hand. Section 3 describes the methodology used to determine the main physical properties (effective radius, surface brightness (SB), absolute magnitude, stellar mass and age) of the 32 ETGs. Section 4 presents the KR while Section 5 presents a discussion of the results obtained in Section 4. Section 6 shows the SL and the SM relations while Section 7 places the results in the context of the galaxy formation and evolution scenarios. Section 8 gives the summary.

Throughout this paper, we use a standard cosmology with $H_0 = 70$ Km s^{-1} Mpc^{-1}, $\Omega_m = 0.3$ and $\Omega_\Lambda = 0.7$. All the magnitudes are in the Vega system, unless otherwise specified.

2 SAMPLE SELECTION AND *HST*-NICMOS IMAGING

The sample of ETGs we constructed is composed of 32 galaxies at $1 < z < 2$ selected from different samples and surveys on the basis of their spectroscopic and morphological classification. We restricted our selection to those galaxies having both (i) deep *HST*-NICMOS observations in the F160W filter ($\lambda \sim 1.6\,\mu$m) sampling the rest-frame continuum $0.55 < \lambda_{rest} < 0.85\,\mu$m at $1 < z < 2$ and (ii) spectroscopic confirmation of their redshift and spectral type. On the basis of these criteria, we were able to collect a sample of 32 ETGs. The samples from which they have been extracted are the following.

(i) 10 ETGs at $1.4 < z < 1.9$ have been selected from the GDDS sample (Abraham et al. 2004; McCarthy et al. 2004). According to the spectral classification described in Abraham et al., we selected those galaxies having Class = 001 (eight galaxies), i.e. pure signatures of an evolved stellar population, and two galaxies having signatures of a young population superimposed to the older one (Class = 101 and 011). These galaxies are listed in Table 1 as SA# and have also been recently studied by Damjanov et al. (2008).

(ii) Six ETGs at $z \simeq 1.27$ have been selected from the sample of Stanford et al. (1997) and belong to the cluster RDCS 0848+4453 in the Linx field. Their spectra show absorption features (Ca II H+K, Mg I and Mg II) and spectral break (B2900, D4000) similar to the present-epoch ellipticals (van Dokkum & Stanford 2003; Stanford et al. 1997). These galaxies, listed in Table 1 as CIG#, have also been previously studied by Moriondo, Cimatti & Daddi (2000).

Table 1. The sample of ETGs.

ID	RA	Dec.	Ref.[a]	NIC[b]	$\mu_{\rm lim}$[c]	B	V	R	I	z	J	H	F160W	K
S2F5_109	03 06 21.08	−00 17 58.0	[1]	2	22.1	24.2 ± 0.3	23.5 ± 0.2	21.8 ± 0.1	20.1 ± 0.1	–	18.2 ± 0.1	–	17.75 ± 0.05	16.6 ± 0.1
S7F5_254	13 34 59.64	+16 49 10.7	[1]	2	22.8	25.0 ± 9.0	24.5 ± 9.0	24.0 ± 9.0	23.1 ± 0.7	–	19.8 ± 0.1	–	19.58 ± 0.09	17.8 ± 0.1
S2F1_357	03 06 52.25	−00 00 09.9	[1]	2	22.8	25.0 ± 9.0	24.5 ± 9.0	23.8 ± 0.4	21.5 ± 0.2	–	19.5 ± 0.1	–	19.04 ± 0.07	17.8 ± 0.1
S2F1_389	03 06 28.03	+00 00 31.6	[1]	2	22.8	24.3 ± 0.5	23.7 ± 0.5	23.7 ± 0.5	23.0 ± 0.5	–	20.3 ± 0.2	–	20.08 ± 0.11	18.2 ± 0.1
S2F1_511	03 06 34.04	+00 02 30.9	[1]	2	22.8	25.0 ± 9.0	24.5 ± 9.0	24.0 ± 9.0	21.6 ± 0.6	–	19.8 ± 0.1	–	19.37 ± 0.08	18.1 ± 0.1
S2F1_142	03 06 36.51	−00 03 01.0	[1]	2	22.8	25.0 ± 9.0	24.5 ± 9.0	23.8 ± 0.3	21.5 ± 0.2	–	19.6 ± 0.1	–	19.00 ± 0.06	17.8 ± 0.1
S7F5_45	13 34 24.98	+16 45 48.6	[1]	2	22.8	–	24.2 ± 0.4	23.5 ± 0.3	22.2 ± 0.3	–	19.6 ± 0.1	–	18.59 ± 0.06	17.6 ± 0.1
S2F1_633	03 06 35.10	+00 04 43.6	[1]	2	22.8	25.0 ± 9.0	24.5 ± 9.0	24.0 ± 9.0	22.5 ± 0.5	–	20.0 ± 0.1	–	19.32 ± 0.08	18.2 ± 0.1
S2F1_443	03 06 31.76	+00 01 13.4	[1]	2	22.8	25.0 ± 9.0	24.5 ± 9.0	24.0 ± 9.0	23.2 ± 0.6	–	20.5 ± 0.1	–	19.69 ± 0.10	18.4 ± 0.1
S2F1_527	03 06 43.34	+00 02 44.8	[1]	2	22.8	25.0 ± 9.0	24.5 ± 9.0	24.0 ± 9.0	22.6 ± 0.4	–	20.4 ± 0.2	–	19.80 ± 0.10	18.3 ± 0.1
SA12-5592	12 05 22.13	−07 24 32.6	[2]	3	24.4	26.79 ± 0.4	25.00 ± 0.09	24.11 ± 0.04	23.24 ± 0.04	23.74 ± 0.2	–	20.01 ± 0.2	20.40 ± 0.16	19.42 ± 0.20
SA12-5869	12 05 21.55	−07 24 09.4	[2]	3	24.4	26.90 ± 9.0	25.85 ± 0.14	24.39 ± 0.05	23.25 ± 0.04	23.78 ± 0.2	–	19.25 ± 0.1	19.64 ± 0.13	18.58 ± 0.13
SA12-6072	12 05 12.58	−07 23 56.5	[2]	3	24.4	26.17 ± 0.2	25.37 ± 0.09	25.26 ± 0.09	24.10 ± 0.08	24.00 ± 9.0	–	20.83 ± 0.3	21.06 ± 0.19	19.79 ± 0.24
SA12-8025	12 05 25.40	−07 21 24.5	[2]	3	24.4	26.54 ± 0.3	25.35 ± 0.09	24.55 ± 0.05	23.16 ± 0.04	22.98 ± 0.1	–	19.83 ± 0.2	19.94 ± 0.14	18.91 ± 0.15
SA12-8895	12 05 14.33	−07 20 14.5	[2]	3	24.4	26.02 ± 0.2	24.67 ± 0.05	23.92 ± 0.03	23.12 ± 0.04	22.95 ± 0.1	–	19.50 ± 0.1	19.44 ± 0.09	18.48 ± 0.12
SA15-4367	15 23 42.63	−00 07 11.7	[2]	3	24.4	26.50 ± 9.0	25.59 ± 0.12	25.03 ± 0.07	23.58 ± 0.05	22.92 ± 0.1	–	21.10 ± 9.0	20.75 ± 0.16	19.47 ± 0.12
SA15-5005	15 23 45.96	−00 06 21.3	[2]	3	24.4	26.50 ± 9.0	25.09 ± 0.09	24.55 ± 0.06	23.59 ± 0.05	23.13 ± 0.2	–	19.90 ± 0.3	20.59 ± 0.15	19.59 ± 0.14
SA15-7543	15 23 44.83	−00 03 37.6	[2]	3	24.4	26.50 ± 9.0	25.77 ± 0.14	24.97 ± 0.06	23.62 ± 0.06	22.73 ± 0.1	–	19.75 ± 0.2	19.70 ± 0.10	19.03 ± 0.10
SA22-0189	22 17 47.59	+00 13 27.1	[2]	3	24.4	99.99 ± 9.0	25.68 ± 0.13	99.99 ± 9.99	22.80 ± 0.04	22.24 ± 0.1	–	19.19 ± 0.05	19.27 ± 0.12	18.05 ± 0.11
SA22-1983	22 17 48.41	+00 16 08.8	[2]	3	24.4	99.99 ± 9.0	25.89 ± 0.13	99.99 ± 9.99	23.68 ± 0.09	23.28 ± 0.2	–	19.98 ± 0.1	20.02 ± 0.19	19.06 ± 0.19
CIG_237	08 48 30.79	+44 53 34.8	[3,4]	3	24.7	26.3 ± 0.1	–	24.7 ± 0.10	–	–	21.59 ± 0.12	20.4 ± 0.09	20.38 ± 0.09	19.53 ± 0.06
CIG_65	08 48 32.42	+44 53 35.1	[3,4]	3	24.7	26.7 ± 0.2	–	24.0 ± 0.05	–	–	20.13 ± 0.03	18.9 ± 0.03	18.71 ± 0.04	18.11 ± 0.02
CIG_142	08 48 32.99	+44 53 46.6	[3,4]	3	24.7	27.4 ± 0.3	–	24.8 ± 0.09	–	–	20.77 ± 0.06	19.7 ± 0.05	19.67 ± 0.08	18.90 ± 0.03
CIG_70	08 48 35.99	+44 53 36.1	[3,4]	3	24.7	26.8 ± 0.2	–	24.2 ± 0.05	–	–	20.25 ± 0.03	19.1 ± 0.03	18.76 ± 0.04	18.14 ± 0.02
CIG_108	08 48 36.16	+44 54 17.3	[3,4]	3	24.7	27.1 ± 0.2	–	24.3 ± 0.06	–	–	20.41 ± 0.04	19.4 ± 0.04	18.91 ± 0.06	18.47 ± 0.02
CIG_135	08 48 36.24	+44 53 55.4	[3,4]	3	24.7	27.4 ± 0.3	–	25.1 ± 0.11	–	–	20.99 ± 0.05	20.0 ± 0.05	19.37 ± 0.08	18.86 ± 0.03
HDF_1031	12 36 40.01	+62 12 07.3	[5]	3	24.3	24.75	23.43	–	21.82	–	–	–	19.57 ± 0.11	–
HDF_1523	12 36 44.39	+62 11 33.1	[5]	3	24.3	25.39	22.95	–	20.87	–	–	–	18.00 ± 0.04	–
HDF_ 731	12 36 44.11	+62 12 44.8	[5]	3	24.3	27.83	25.92	–	24.61	–	–	–	20.24 ± 0.14	–
HUDF_472	03 32 38.12	−27 47 49.6	[6,7]	3	25.1	28.2 ± 0.2	26.12 ± 0.03	24.92 ± 0.01	–	23.83 ± 0.01	22.21 ± 0.07	–	20.93 ± 0.08	19.81
HUDF_996	03 32 36.92	−27 46 28.5	[6,7]	3	25.1	27.7 ± 0.1	26.56 ± 0.04	24.87 ± 0.01	–	23.80 ± 0.01	22.47 ± 0.07	–	21.42 ± 0.08	19.35
53W091	17 22 32.69	+50 06 01.9	[8]	2	22.9	–	–	24.5 ± 0.2	23.7 ± 0.03	–	21.8 ± 0.03	19.5 ± 0.1	19.64 ± 0.04	18.7 ± 0.1

Notes. The magnitudes are in the Vega system. [a]References for the single objects. [1] Longhetti et al. (2007); [2] Abraham et al. (2004); [3] Stanford et al. (1997); [4] Moriondo et al. (2000); [5] Stanford et al. (2004); [6] Cimatti et al. (2008); [7] Daddi et al. (2005) and [8] Dunlop et al. (1996).

[b]NICMOS camera used: 2 for NIC2 and 3 for NIC3. The plate scale of the NIC2 camera is 0.075 arcsec pixel^{-1} and the plate scale of the NIC3 camera is 0.2 arcsec pixel^{-1}. HUDF images have been drizzled to 0.09 arcsec pixel^{-1}.[c]Limiting SB (mag arcsec^{-2}) at 1σ in the F160W band measured on the NICMOS images.

(iii) Three ETGs at $1 < z < 1.8$ have been selected from the sample of Stanford et al. (2004) in the *Hubble Deep Field*-North (HDF-N) according to their spectral type ST < 0.1 characterizing an old and passive population of stars and on their morphology. They are listed as HDF_#.

(iv) Two ETGs (HUDF_#) at $z \simeq 1.4$ and at $z \simeq 1.9$, respectively, have been selected from the sample of Cimatti et al. (2008; see also Daddi et al. 2005) in the Hubble Ultra Deep Field (HUDF). They are classified as early-types on the basis of both their morphology and their spectral features.

(v) The ETG 53W091 has been taken from Dunlop et al. (1996; see also Spinrad et al. 1997). The spectrum of this galaxy is characterized by absorption features typical of an old stellar population and its light profile is bulge dominated (Waddington et al. 2002).

(vi) The remaining 10 ETGs (S2F# and S7F#) come from our own sample of ETGs spectroscopically classified at $1.2 < z < 1.7$ in the framework of the TESIS project (Saracco et al. 2003, 2005). The study of their spectrophotometric properties and of their morphology based on multiwavelength data and *HST*-NICMOS observations is described in previous work (Longhetti et al. 2005, 2007).

The whole sample of 32 ETGs is listed in Table 1 where we also report for each galaxy the photometry in different bands. All the magnitudes, with the exception of the F160W-band magnitude, are taken from the literature as quoted in Column 4 of the table. The magnitude in the F160W filter is the SEXTRACTOR MAG_BEST magnitude (Bertin & Arnouts 1996) that we estimated from the *HST*-NICMOS images we retrieved from the *HST* archive. All the magnitudes are in the Vega system. Given the different samples the galaxies have been extracted from, the wavelength coverage is not the same for all the galaxies as well as the filters used. We did not convert the magnitudes derived in slightly different filters from the different surveys to a common filter system since we would have introduced large and possibly systematic errors. We have preferred to keep the original magnitudes as given by the authors and to use the appropriate set of response filter functions in our analysis. We describe the multiwavelength coverage and the filters used in the various surveys in Appendix A.

The median redshift of the sample thus collected is $z_{\rm med} = 1.45$. *HST*-NICMOS images with the NIC2 (0.075 arcsec pixel^{-1}) camera are available for the 10 galaxies of our sample and for the galaxy 53W091, i.e. for ∼30 per cent of the sample. For the remaining galaxies, the available images are based on NIC3 (0.2 arcsec pixel^{-1}) camera. The NIC3 images relevant to the two galaxies in the HUDF were drizzled to 0.09 arcsec pixel^{-1}. The 1σ limiting SB $\mu_{\rm lim}$ of the different NICMOS images is reported in Table 1. The NICMOS mosaics for the whole sample of ETGs can be retrieved at the web page http://www.brera.inaf.it/utenti/saracco/.

3 PHYSICAL PARAMETERS OF EARLY-TYPE GALAXIES

3.1 Morphological parameters

We derived the effective radius $r_{\rm e}$ (arcsec) and the mean SB $\langle\mu\rangle_{\rm e}$ (mag arcsec^{-2}) within $r_{\rm e}$ of our galaxies from the NICMOS images by fitting a Sérsic profile (Sérsic 1968) to the observed light profiles. The analytic expression of the adopted profiles is

$$I(r) = I_{\rm e} \exp\left\{-b_n\left[(r/r_{\rm e})^{1/n} - 1\right]\right\}, \quad (1)$$

where $n = 4$ and $n = 1$ values define the de Vaucouleurs (de Vaucouleurs 1948) and the exponential (disc) profiles, respectively. We used GALFIT software (v. 2.0.3; Peng et al. 2002) to perform the fitting to the observed profiles. The bi-dimensional Sérsic model has been convolved with the point spread function (PSF) of the NIC2 and the NIC3 cameras modelled by means of the TINY TIM[1] (v. 6.3) software package (Krist 1995; Krist & Hook 2004). The fitting provided us with the semimajor axis $a_{\rm e}$ of the projected elliptical isophote containing half of the total light and with the axial ratio b/a. We thus derived the circularized effective radius $r_{\rm e} = a_{\rm e}\sqrt{b/a}$.

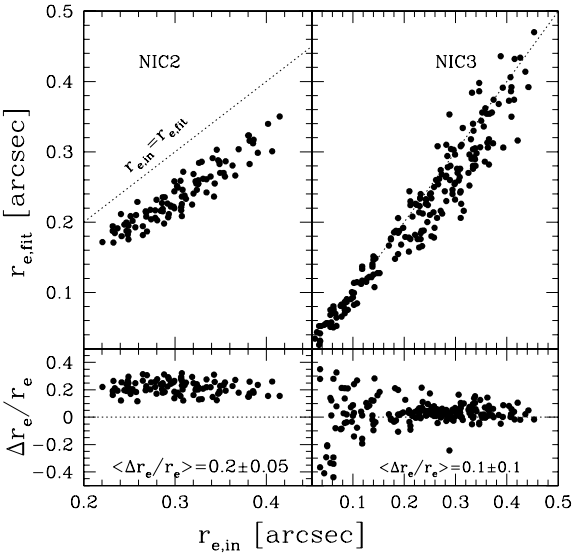

Figure 1. Comparison between the effective radius of the simulated galaxies ($r_{\rm e,in}$) and the effective radius $r_{\rm e,fit}$ obtained through the fitting with the Sérsic profile for the NIC2 (left-hand panel) and the NIC3 (right-hand panel) images.

To assess the robustness and the accuracy of our estimate of the effective radius of galaxies, we applied the same fitting procedure to a set of simulated galaxies inserted in the real background. The simulations follow those described in details in Longhetti et al. (2007) for the NIC2 images. Here, we summarize the main features of the procedure followed to obtain the simulated observations. We generated with GALFIT a set of 100 galaxies described by a de Vaucouleurs profile with axial ratio b/a and position angle (PA) randomly assigned in the ranges $0.4 < b/a < 1$ and $0 < {\rm PA} < 180^\circ$, respectively. Magnitudes in the F160W filter were assigned randomly in the range $18 <$ F160W < 21. Effective radii $r_{\rm e,in}$ were assigned randomly in the ranges $0.2 < r_{\rm e,in} < 0.5$ arcsec (corresponding to 1.5–4 kpc at $z \simeq 1$) for the NIC2 images. In order to verify the absence of a bias against the detection of small effective radii ($r_{\rm e,in} < 0.2$ arcsec, $R_{\rm e} < 1.5$ Kpc) in the fitting of galaxies in the NIC3 images characterized by a pixel scale of 0.2 arcsec pixel^{-1}, we also simulated here a set of galaxies with $0.05 < r_{\rm e,in} < 0.2$ arcsec. The simulated galaxies have been convolved with the NICMOS PSFs and then embedded in the real NIC2 and NIC3 images. We used the simulations described in Longhetti et al. (2007) for the NIC2 galaxies and the images relevant to the sample of McCarthy et al. (2004) to simulate the NIC3 galaxies. We then fit the simulated galaxies with the Sérsic profile and studied the behaviour of the resulting $r_{\rm e,fit}$ checking our ability in recovering the input value $r_{\rm e,in}$. In Fig. 1, we plot the values of the effective

[1] www.stsci.edu/software/tinytim

Table 2. Morphological parameters of galaxies. The effective radii obtained by fitting the Sérsic profile and the resulting surface brightnesses take into account the correction for the underestimate of r_e derived from the simulations (see Section 3.1). We applied a correction of 0.07 arcsec to the NIC2 data and of 0.03 arcsec to the NIC3 data. The error on the effective radii takes into account both the formal error of the profile fitting and the rms observed in recovering the intrinsic radius of simulated galaxies, namely $\sigma_{r_e}^{\rm NIC2} = 0.02$ arcsec and $\sigma_{r_e}^{\rm NIC3} = 0.04$ arcsec. The magnitude F160W$_{\rm tot}$ is the total magnitude of the best-fitting profile as derived by GALFIT. The effective radius $r_e^{\rm others}$ is the original effective radius estimated by other groups.

Object	z	F160W$_{\rm tot}$ (mag)	M_R (mag)	r_e (arcsec)	$r_e^{\rm others}$ (arcsec)	R_e (Mpc)	$\langle\mu\rangle_e^R$ (mag arcsec^{-2})	$\langle\mu\rangle_e^{\rm F160W}$ (mag arcsec^{-2})	*Age* (Gyr)	$\mathcal{M}_*$ (10^{11} M$_\odot$)
S2F5_109	1.22	17.47 ± 0.02	-24.86	0.53 ± 0.02	–	4.4 ± 0.2	20.1 ± 0.1	18.1 ± 0.1	3.5	7.6
S7F5_254	1.22	19.46 ± 0.03	-22.91	0.27 ± 0.02	–	2.3 ± 0.2	20.8 ± 0.2	18.6 ± 0.2	4.5	3.9
S2F1_357	1.34	18.72 ± 0.03	-23.71	0.33 ± 0.02	–	2.8 ± 0.2	20.4 ± 0.2	18.3 ± 0.2	4.2	4.9
S2F1_389	1.40	19.79 ± 0.03	-22.73	0.25 ± 0.03	–	2.1 ± 0.3	20.8 ± 0.2	18.7 ± 0.2	3.5	1.8
S2F1_511	1.40	19.15 ± 0.03	-23.64	0.25 ± 0.02	–	2.1 ± 0.2	20.1 ± 0.2	18.1 ± 0.2	1.0	0.9
S2F1_142	1.43	18.65 ± 0.03	-24.00	0.36 ± 0.02	–	3.1 ± 0.2	20.5 ± 0.2	18.4 ± 0.2	3.5	4.1
S7F5_45 \	1.45	18.83 ± 0.03	-23.89	0.55 ± 0.03	–	4.7 ± 0.3	21.5 ± 0.1	19.5 ± 0.1	1.0	2.0
S2F1_633	1.45	19.00 ± 0.03	-23.67	0.31 ± 0.02	–	2.6 ± 0.2	20.5 ± 0.2	18.5 ± 0.2	2.6	2.5
S2F1_443	1.70	19.44 ± 0.03	-23.76	0.40 ± 0.03	–	3.4 ± 0.3	21.4 ± 0.2	19.4 ± 0.2	3.2	3.4
S2F1_527	1.35	19.50 ± 0.03	-23.38	0.20 ± 0.03	–	1.7 ± 0.3	20.2 ± 0.2	18.0 ± 0.2	2.3	1.1
SA12-5592	1.623	20.30 ± 0.01	-22.85	0.16 ± 0.04	0.05 ± 0.05	1.4 ± 0.3	20.50 ± 0.4	18.36 ± 0.4	0.9	0.3
SA12-5869	1.510	19.53 ± 0.02	-23.20	0.34 ± 0.04	0.25 ± 0.06	2.8 ± 0.3	21.29 ± 0.3	19.16 ± 0.3	1.2	0.4
SA12-6072	1.576	20.96 ± 0.01	-22.11	0.16 ± 0.04	0.09 ± 0.04	1.4 ± 0.3	21.12 ± 0.4	18.98 ± 0.4	1.4	0.3
SA12-8025	1.397	19.87 ± 0.01	-22.92	0.30 ± 0.04	0.24 ± 0.03	2.4 ± 0.3	21.31 ± 0.3	19.18 ± 0.3	3.7	0.5
SA12-8895	1.646	19.20 ± 0.02	-23.84	0.46 ± 0.04	0.50 ± 0.05	3.9 ± 0.3	21.66 ± 0.2	19.56 ± 0.2	0.8	0.7
SA15-4367	1.725	20.61 ± 0.01	-22.64	0.30 ± 0.04	0.22 ± 0.03	2.5 ± 0.3	22.16 ± 0.3	20.05 ± 0.3	0.9	0.4
SA15-5005	1.845	20.46 ± 0.01	-22.97	0.25 ± 0.04	0.21 ± 0.03	2.1 ± 0.3	21.59 ± 0.3	19.42 ± 0.3	0.9	0.4
SA15-7543	1.801	19.64 ± 0.01	-23.80	0.39 ± 0.04	0.48 ± 0.08	3.3 ± 0.3	21.77 ± 0.2	19.60 ± 0.2	1.0	0.9
SA22-0189	1.490	19.19 ± 0.01	-23.76	0.38 ± 0.04	0.37 ± 0.03	3.2 ± 0.3	21.21 ± 0.2	19.08 ± 0.2	3.5	1.8
SA22-1983	1.488	20.03 ± 0.02	-22.78	0.17 ± 0.04	0.09 ± 0.04	1.5 ± 0.3	20.36 ± 0.4	18.23 ± 0.4	3.7	1.0
CIG_237	1.271	20.14 ± 0.03	-22.50	0.35 ± 0.07	0.29 ± 0.02	3.0 ± 0.6	21.96 ± 0.4	19.89 ± 0.4	3.5	0.3
CIG_65	1.263	18.85 ± 0.01	-24.18	0.39 ± 0.04	–	3.3 ± 0.3	20.89 ± 0.2	18.82 ± 0.2	4.2	2.1
CIG_142	1.277	19.63 ± 0.02	-23.21	0.19 ± 0.05	0.14 ± 0.02	1.6 ± 0.4	20.06 ± 0.6	17.99 ± 0.6	4.2	1.0
CIG_70	1.275	18.02 ± 0.01	-24.12	1.70 ± 0.60	1.10 ± 0.13	13.9 ± 5.0	23.19 ± 0.8	21.12 ± 0.8	4.2	2.1
CIG_108	1.277	18.48 ± 0.02	-23.97	1.00 ± 0.30	0.79 ± 0.08	8.4 ± 2.5	22.56 ± 0.6	20.49 ± 0.6	4.2	1.4
CIG_135	1.276	19.33 ± 0.02	-23.52	0.56 ± 0.05	0.68 ± 0.07	4.7 ± 0.4	22.15 ± 0.2	20.08 ± 0.2	4.3	0.9
HDF_1031	1.015	19.37 ± 0.03	-22.47	0.26 ± 0.02	0.21	2.1 ± 0.2	20.52 ± 0.2	18.42 ± 0.2	1.1	0.2
HDF_1523	1.050	17.67 ± 0.02	-24.13	0.59 ± 0.10	0.60	4.8 ± 0.8	20.62 ± 0.4	18.52 ± 0.4	2.0	2.1
HDF_ 731	1.755	20.20 ± 0.05	-23.21	0.55 ± 0.09	0.63	4.6 ± 0.8	23.08 ± 0.4	20.92 ± 0.4	1.4	0.4
HUDF_472	1.921	20.99 ± 0.03	-22.75	0.20 ± 0.06	0.10(0.08)[a]	1.7 ± 0.5	21.65 ± 0.7	19.48 ± 0.7	0.8	0.4
HUDF_996	1.390	21.43 ± 0.05	-21.43	0.22 ± 0.06	0.31(0.10)[a]	1.8 ± 0.5	22.24 ± 0.6	20.13 ± 0.6	1.3	0.1
53W091	1.55	19.77 ± 0.04	-23.37	0.19 ± 0.02	0.30 ± 0.08	1.6 ± 0.2	20.33 ± 0.3	18.19 ± 0.3	2.4	0.6

[a]These values have been derived from *HST*-ACS observations in the F850W filter. The values out of the brackets have been derived from Daddi et al. (2005) and those within the brackets from Cimatti et al. (2008).

radius $r_{e,\rm fit}$ versus $r_{e,\rm in}$ in the case of NIC2 and NIC3 images. It can be seen that in the NIC2 images the effective radius of the galaxies is slightly underestimated by $\Delta r_e^{\rm NIC2} \simeq 0.07$ arcsec on average, while in the NIC3 images the mean underestimate is $\Delta r_e^{\rm NIC3} \simeq 0.03$ arcsec. The rms measured is 0.04 arcsec in the NIC3 images and 0.02 arcsec in the NIC2 images and are much larger than the formal fitting error on the effective radius. Thus, our fitting tends to slightly underestimate the effective radius r_e. Fig. 1 also shows that the pixel scale of NIC3 does not represent a limit in the detection of small effective radii and thus that no bias is present in our analysis against very small galaxies. The small underestimate of r_e has been taken into account in the following analysis and in the derivation of the mean surface brightnesses by adding the mean offset Δr_e quoted above to the best-fitting values r_e. In Table 2, we report the morphological parameters r_e (arcsec) and R_e (Kpc) derived from the fitting to the profile of our galaxies and the mean SB in the F160W band

$$\langle\mu\rangle_e^{\rm F160W} = {\rm F160W_{tot}} + 5\log(r_e) + 2.5\log(2\pi), \quad (2)$$

where F160W$_{\rm tot}$ is the total magnitude in this filter derived by GALFIT and reported in Table 2.

The morphology for some of them, namely the CIG# galaxies, the HDF# galaxies and 53W091, had been already derived in the rest-frame *R* band from Moriondo et al. (2000), Stanford et al. (2004) and Waddington et al. (2002), respectively. Our new estimates are in good agreement with their estimates in spite of the different method used to fit the profiles. For four galaxies of our sample, namely HUDF_472, HUDF_996, HDF_1031 and HDF_1523, the estimate of the effective radius derived from *HST* images in the optical bands (F814W and F850W filters) sampling the rest-frame wavelength $\lambda_{\rm rest} < 4000$ Å is also available from the literature. In the case of the two galaxies in the HDF at $z \sim 1$, the estimates of R_e we derived from the NICMOS images agree well with those derived by van Dokkum et al. (2003) from observations in the F814W filter. Our estimate of R_e for the galaxy HUDF_996 agrees with the one of Daddi et al. (2005) made on the F850W image while it is a factor of 2 of the estimate of Cimatti et al. (2008). For the galaxy HUDF_472 at $z \sim 1.9$, our estimate is a factor of 2 of the estimate of both Daddi et al. (2005) and Cimatti et al. (2008). It should be noted that, given the redshift of this latter galaxy, the filters F850W and F160W sample the profile at $\lambda_{\rm rest} \simeq 2900$ Å and at $\simeq$5700 Å respectively, two wavelength ranges which differ substantially for the

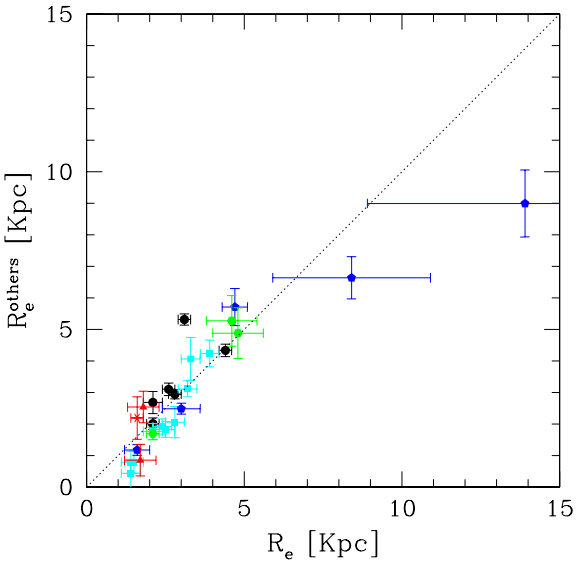

Figure 2. Comparison between the effective radius R_e (Kpc) we obtained from the analysis of the NICMOS images and the one obtained by the other groups R_e^{others}. Cyan squares are the SA# ETGs compared with the estimates of Damjanov et al. (2008); blue pentagons are the CIG# ETGs in the RDCS 0848+4453 compared with the estimates of Moriondo et al. (2000); green hexagon are the HDF# ETGs compared with the estimates of Stanford et al. (2004); red triangles are the HUDF# ETGs compared with the ACS-based estimates of Cimatti et al. (2008); red starred symbol is 53W091 compared with the estimate of Waddington et al. (2002) and the black points are six out of the 10 galaxies studied in Longhetti et al. (2007) compared with the recent estimates of Damjanov et al. (2008).

contribution from the young and the old stars, respectively. Thus, in this case the different estimates could reflect a real difference of the galaxy profile if observed at such different wavelengths (e.g. McGrath et al. 2008). However, we note that the bi-dimensional fit to the observed images of the two HUDF galaxies (together with those of the two RDCS galaxies with $R_e > 8$ Kpc) presents significant residuals and thus their derived R_e could be affected by large errors. The 10 SA# galaxies selected from the GDDS sample have been recently studied by Damjanov et al. (2008). We note that the effective radii they derive are systematically smaller than ours and that for three galaxies they derive effective radii as small as 0.3, 0.4 and 0.7 Kpc, respectively, while we never obtain effective radii smaller than 1 Kpc. In Fig. 2, the comparison between the original estimate of the effective radii R_e^{others} (Kpc) obtained by the other groups and our new estimate is shown. The different symbols refer to the different data sets as detailed in the caption of the figure. The original estimate of the effective radii R_e^{others} (arcsec) as derived by the other groups is also reported in Table 2.

3.2 Absolute magnitudes, stellar masses and age

For each galaxy of the sample, we derived the *R*-band absolute magnitude M_R, the stellar mass $\mathcal{M}_*$ and the mean age *Age* of the stellar population. We made use of the stellar population synthesis models of S. Charlot & G. Bruzual (in preparation, hereafter referred to as CB08) and of the best-fitting code HYPERZ (Bolzonella, Miralles & Pellò 2000) to find the best-fitting template to the observed spectral energy distribution (SED) at the redshift of each galaxy. The set of templates considered includes three SFHs described by an exponentially declining star formation rate (SFR) $\propto e^{-t/\tau}$ with e-folding time $\tau = [0.1, 0.3, 0.6]$ Gyr and two metallicity $0.4\,Z_\odot$ and $Z_\odot$. We assumed Chabrier initial mass function (IMF; Chabrier 2003). Extinction A_V has been considered and treated as a free parameter in the fitting. We adopted the extinction curve of Calzetti et al. (2000) and allowed A_V to vary in the range $0 \leq A_V \leq 0.6$. For 24 out of the 32 galaxies, the best-fitting template is defined by SFHs with $\tau \leq 0.3$ Gyr and $A_V \leq 0.3$.

The *R*-band absolute magnitude M_R has been derived from the observed flux in the F160W filter since it samples the *R* band in the rest frame of the galaxies. To derive M_R, we used the relation

$$M_R(z) = \mathrm{F160W_{tot}} - 5\log[D_\mathrm{L}(z)] - k_{R,\mathrm{F160W}}(z), \quad (3)$$

where $\mathrm{F160W_{tot}}$ is the total magnitude, $D_\mathrm{L}(z)$ is the luminosity distance (Mpc) at the redshift z of the galaxy and $k_{R,\mathrm{F160W}}(z)$ is the colour *k*-correction term defined as

$$k_{R,\mathrm{F160W}} = [R(z=0) - \mathrm{F160W}(z)]_\mathrm{temp}, \quad (4)$$

where the two magnitudes $R(z=0)$ and $F160W(z)$ are derived from the best-fitting template at $z = 0$ and redshifted at the redshift of the galaxy, respectively. The uncertainty affecting this *k*-correction is typically comparable or smaller than the photometric errors since the filter F160W is extremely close to the rest-frame *R* band over the whole redshift range considered and thus the dependence in the best-fitting template tends to vanish. Indeed, we have verified that even considering the oldest template among the best-fitting templates (the one 4.0 Gyr old) and the youngest template (1 Gyr old), the difference between the *k*-correction is less than 0.15 mag over the whole redshift range considered. Thus, even hypothesizing to fail the fit to the observed SED of a galaxy we would wrong its absolute magnitude by no more than 0.1 mag. For this reason, we consider our estimate of the *R*-band absolute magnitude of our galaxies extremely reliable.

The stellar mass $\mathcal{M}_*$ of the galaxies we derived is the one usually computed in the literature and it is given by the equation

$$\mathcal{M}_* = 2 \times 10^{-17} b 4\pi D_\mathrm{L}^2(z) \mathcal{M}_*^\mathrm{model}/\mathrm{L}_\odot, \quad (5)$$

where *b* is the normalization factor of the best-fitting model provided by HYPERZ and $\mathcal{M}_*^\mathrm{model}$ is the mass associated to the best-fitting template considering only the stellar mass still locked into stars. This quantity is listed in column 7 of the .4color files of CB08 models. The mass we derived is the mass locked into stars at the epoch of their observation after the gas fraction returned to the interstellar medium. This mass is typically about 60 per cent the one derived including the gas return fraction, i.e. the one obtained by integrating the SFR over the age of the galaxy. A detailed comparison between different stellar mass estimators is given by Longhetti & Saracco (2008) which also provide the relations to convert an estimate to another accounting for different IMFs. The uncertainty affecting our stellar mass estimate depends mainly on the uncertainty affecting the SFH (τ) and the age of the best-fitting model and on the best-fitting parameter A_V, three parameters tightly linked among them. The SFH and the age mainly affect the value of M_*^model while the extinction A_V affect mainly the normalization *b* of the fit. Since we deal with galaxies of known spectral type and redshift, the best-fitting SFH and age are sharply constrained producing negligible differences in the values of M_*^model. For instance, even considering the youngest and the oldest ages possible in this range of redshift, i.e. 1 and 4 Gyr, the corresponding M_*^model for the same SFH would differ only by a factor of 1.15. On the contrary, the normalization *b* of the model, which is a free parameter in the fitting, can vary up to a factor of ∼2

since it depends on the photometric accuracy in the various bands, on the number of photometric points sampling the spectrum of the galaxy and on the free parameter A_V. Thus, the internal accuracy of our stellar mass estimates is within a factor of 2 and it is two times the uncertainty affecting the absolute magnitudes. This internal error does not consider the possible systematics due to different IMFs (e.g. Salpeter IMF provides higher stellar masses than Kroupa and Chabrier IMFs) or different library models (see e.g. Maraston et al. 2006; Longhetti et al. 2008). Thus, for a comparison with other samples, such possible systematics should be taken into account by scaling, if necessary, the different estimates. Systematics and scaling relations among different library codes can be found in Longhetti et al. (2008).

The mean age of the best-fitting model depends both on the SFHs and on the A_V in the way that higher A_V and shorter SFHs provide younger best-fitting models for a given observed SED. As previously said, most of the galaxies (24 out of 32) are best fitted by the shorter SFHs considered, i.e. by models with $\tau \leq 0.3$ Gyr and $A_V \leq 0.3$ suggesting that the best fitting does not tend toward either old or young models (old with respect to the age of the universe at the redshift of the galaxy). However, the main degeneracy is between the age of the best-fitting model and the extinction A_V. Indeed, while two different SFHs, for instance the one with $\tau \leq 0.1$ and the other with $\tau \leq 0.3$, account for differences in the best-fitting age of the order of few tenth of Gyr, different values of A_V even within the range $0 < A_V < 0.6$ can produce differences as large as 1 Gyr. An old stellar population can, in fact, be fitted by a young model reddened by an extinction $A_V > 0$. In order to verify the absence of any systematics in our results due to the best-fitting procedure, we have compared the values of the extinction A_V with the age of the best-fitting template. In Fig. 3, we plot A_V as a function of the age of the best-fitting model for the sample of 32 ETGs. No systematics are present among the two parameters confirming that young best-fitting templates are not a faked result of the fitting procedure. It is worth noting that, with the exception of two galaxies of the GDDS sample, our estimate of the ages agrees within ∼0.3 Gyr (0.5 Gyr for the old ones) with the ages derived by the various authors from the spectral features of the galaxies.

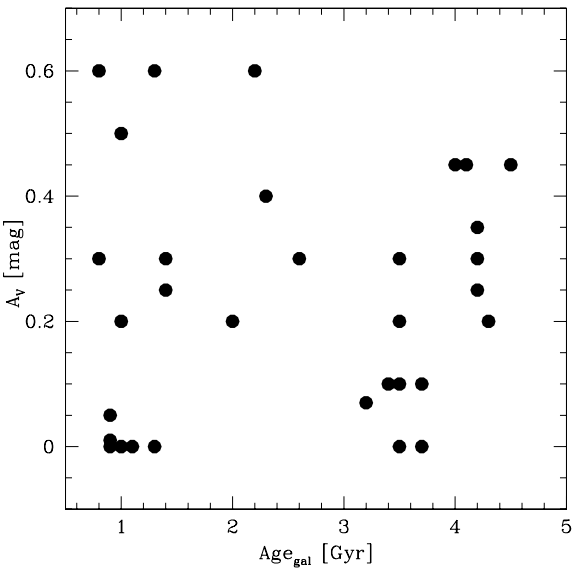

Figure 3. The extinction A_V is plotted as a function of the mean age Age_gal of the best-fitting model for the sample of 32 ETGs. No systematics are present between the two parameters.

In Table 2, we report for each galaxy the R-band absolute magnitude, the stellar mass and the mean age derived for each galaxy from the best fitting to the photometry.

4 THE EVOLUTION OF THE KORMENDY RELATION

The KR (Kormendy 1977) is a linear scaling relation between the logarithm of the effective radius R_e (Kpc), i.e. the radius containing half of the light, and the mean SB $\langle\mu\rangle_e$ (mag arcsec^{-2}):

$$\langle\mu\rangle_e = \alpha + \beta \log(R_e). \quad (6)$$

The ETGs follow this relation with a fixed slope $\beta \sim 3$ up to $z \sim 1$ (e.g. di Serego Alighieri et al. 2005) while the zero-point α varies with the redshift reflecting the evolution that the galaxy underwent.

In Fig. 4 (left-hand panel), the values of R_e and $\langle\mu\rangle_e^R$ in the R band for the 32 galaxies at $1 < z < 2$ derived as described in the previous section are plotted on the (μ_e,R_e) plane. The values of $\langle\mu\rangle_e^R$ have been corrected for the cosmological dimming factor $(1+z)^4$. We converted the SB $\langle\mu\rangle_e^{F160W}$ in the F160W filter into that in the rest-frame R band $\langle\mu\rangle_e^R$ applying to each galaxy the k-correction $k_{R,F160W}$ described in Section 3.2. In Fig. 4, the observed KR in the R band at $z \sim 0$ (see La Barbera et al. 2003),

$$\langle\mu\rangle_e = 18.2 + 2.92 \log(R_e), \qquad z = 0, \quad (7)$$

is also shown (thin black line). The thick (red) solid line is the KR we obtain from the best fitting of our sample

$$\langle\mu\rangle_e = 16.1^{+0.1}_{-0.2} + 2.72^{+0.5}_{-0.2} \log(R_e), \qquad 1 < z < 2, \quad (8)$$

and the two thick dashed lines represent the dispersion at 1σ of the relation. It can be seen that the slope β of the KR we fit at $z \sim 1.5$ does not change significantly with respect to the KR at $z = 0$, while we detect a significant evolution of the zero-point α which changes more than 2 mag in this redshift range. Thus, at least up to $z \sim 1.5$–2, ETGs tend to distribute on the (μ_e, R_e) plane according to a KR with a slope similar to the one of local ETGs $z = 0$. The different zero-point accounts for the evolution which the galaxies undergo and tell us that in case of pure luminosity evolution, i.e. at constant R_e, galaxies must evolve by more than 2 mag in the rest-frame R band from $z_{mean} \sim 1.5$ to $z = 0$, in agreement with previous results (see e.g. McIntosh et al. 2005; Longhetti et al. 2007; Cimatti et al. 2008). Such evolution exceeds almost 1 mag the one expected assuming an average passive luminosity evolution for the whole sample and exceeds much more the evolution inferred from the observed luminosity function of galaxies in this redshift range (e.g. Pozzetti et al. 2003; Zucca et al. 2006; Cirasuolo et al. 2007; Feulner et al. 2007; Marchesini et al. 2007). However, our sample of galaxies is spread over a range of redshift, $1 < z < 2$, which spans about 2.5 Gyr of time, a large interval if compared to the cosmic time at $z \sim 1$ (5.7 Gyr) and at $z \sim 2$ (3.2 Gyr). Thus, in order to assess whether the observed evolution of the zero-point α of the KR can be accounted for by luminosity evolution, we derived for each galaxy its own luminosity evolution $E(z)$ in the rest-frame R band over the interval $\Delta t = t(z = 0) - t(z)$, corresponding to the time elapsed from z to $z = 0$. The evolutionary term $E(z)$ has been calculated taking into account the different ages of the galaxies at the observed redshift as provided by the best-fitting model. Thus, for each galaxy we computed the term $E(z) = [M_R(z) - M_R(z = 0)]_{model}$, i.e. the difference between the R-band absolute magnitude of the best-fitting model with age Age and the R-band magnitude of the same model with age $Age + \Delta t$. This term added to equation (3) provides the SB $\langle\mu\rangle_e^R$ that our galaxies would have at $z = 0$ in the

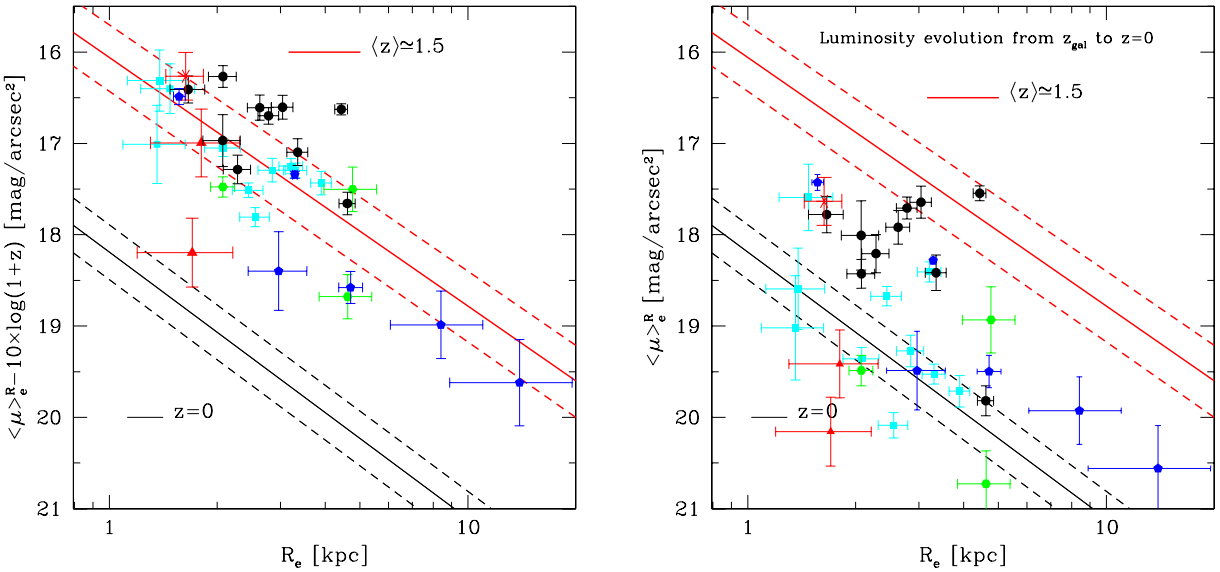

Figure 4. Left-hand panel: mean SB $\langle\mu\rangle_e$ versus effective radius R_e (kpc) for the 32 ETGs of the sample. The thin (black) solid line represents the KR at $z \sim 0$ (equation 7) and the short-dashed lines represent the $\pm 1\sigma$ dispersion of the relation. The thick (red) line is the KR at $z \sim 1.5$ as resulting from the best fit to the sample (equation 8). The short-dashed lines represent the scatter around this relation. All the data have been corrected for the cosmological dimming factor $(1+z)^4$, thus the deviation from the KR at $z = 0$ reflects the evolution of the SB due to the luminosity and/or size evolution of galaxies. Black points are the S2# ETGs (Longhetti et al. 2007), cyan squares are the SA# ETGs from the GDDS sample (McCarthy et al. 2004), blue pentagons are the CIG# ETGs in the RDCS 0848+4453 (Stanford et al. 1997), green hexagon are the HDF# ETGs, red triangles are the HUDF# ETGs (Cimatti et al. 2008) and the red starred symbol is 53W091 (Dunlop et al. 1996). Right-hand panel: mean SB $\langle\mu\rangle_e$ versus effective radius R_e (kpc) for the 32 galaxies of our sample after they have evolved in luminosity. Each galaxy has evolved in luminosity over the interval Δt corresponding to the time elapsed from the redshift z of the galaxy to $z = 0$. The evolution $E(z)$ has been derived accounting for the different age of each galaxy at the observed redshift (see Section 4).

case of pure luminosity evolution. In Fig. 4 (right-hand panel), we show how the 32 ETGs of our sample would be displaced at $z = 0$ in the (μ_e, R_e) plane. {We see that almost half of the sample reaches a SB not exceeding the one derived from the KR at $z = 0$ while the remaining half shows a SB in excess of ∼1 mag with respect to the local KR. In particular, the luminosity evolution brings 11 ETGs on to the KR at $z = 0$ and two ETGs just below it while leaving the remaining 19 ETGs with a SB exceeding much more than 1σ the local KR.} It seems that for a fraction of ETGs at $z > 1$, the expected luminosity evolution is sufficient to account for their SB. They move in the (μ_e, R_e) plane from high to low redshift in agreement with the local KR. On the contrary, for the remaining fraction of ETGs the expected luminosity evolution is not sufficient to dim their SB to the one defined by the local KR. The other parameter involved in the KR relation, the effective radius R_e, must evolve and the hypothesis of fixed size must be rejected for these galaxies. A size evolution of at least a factor of ∼2.5 from $z \sim 1.5$ to 0 is needed to account for the observed SB excess.

5 YOUNG VERSUS OLD ETGs: TWO DISTINCT POPULATIONS AT $z \sim 1.5$?

In the previous section, we have seen that for 13 ETGs the pure luminosity evolution can move them from the KR at $z \simeq 1.5$ on to the KR at $z = 0$, while for the remaining 19 ETGs a different, more complex evolution is required. In fact, this suggests that two distinct populations of ETGs exist at $z \simeq 1.5$. In order to better investigate this evidence, we compared the properties of the 13 ETGs whose luminosity evolution places them on to the KR at $z = 0$ with the remaining 19 ETGs. Basically, the luminosity evolution $E(z)$ derived by models over a given interval Δt of time depends on the SFH and on the age of the best-fitting model. The SFHs which fit the SED of our galaxies are described by e-folding time τ much shorter than the typical Δt over which the luminosity evolution is computed ($\tau \leq 0.3$ Gyr to be compared with $\Delta t \sim 9$ Gyr from $z = 1.5$ to 0). Thus, the slightly different values of τ cannot produce significant differences in $E(z)$ over this interval. Consequently, the other parameter affecting the luminosity evolution, that is the age of the best-fitting model, must be the reason of the different behaviour of the two sub-samples. If so, we expect that the two sub-samples of galaxies show a different age distribution.

In Fig. 5, the age distribution of the 13 galaxies (dashed green histogram), which agree with the KR at $z = 0$, is compared with the age distribution of the remaining 19 ETGs (solid red histogram). It is worth noting that the two sub-samples, with the exception of two ETGs (one for each sub-sample), describe two separated distributions. The first distribution is sharply picked at ∼1 Gyr and the other distribution picks at ∼3.5 Gyr. As shown in Section 3.2, age and extinction A_V are not correlated and no systematics are present between them (see Fig. 3). Moreover, the different values of τ considered cannot account for such different ages. Indeed, a galaxy 1 Gyr old fitted by a SFH $\tau = 0.1$ Gyr would be ∼1.3 Gyr old if fitted with a model $\tau = 0.3$ Gyr. Analogously, a galaxy 4 Gyr old fitted by a SFH $\tau = 0.3$ Gyr would be ∼3.5 Gyr old if fitted with a model $\tau = 0.1$ Gyr. Thus, the two different distributions are not a consequence of the degeneracy between SFH, age and extinction but they reflect real differences among the ETGs: the 13 ETGs which fall on the local KR are, in fact, younger than the remaining 19 ETGs. Given the uncertainties discussed above, it is reliable to consider a mean difference of about 1.5–2 Gyr between the age of the two populations. Hereafter, we will refer to these two populations as young ETGs (yETGs) and old ETGs (oETGs).

In fact, the different age of the stellar populations of the two sub-samples of ETGs is the reason of their different behaviour with

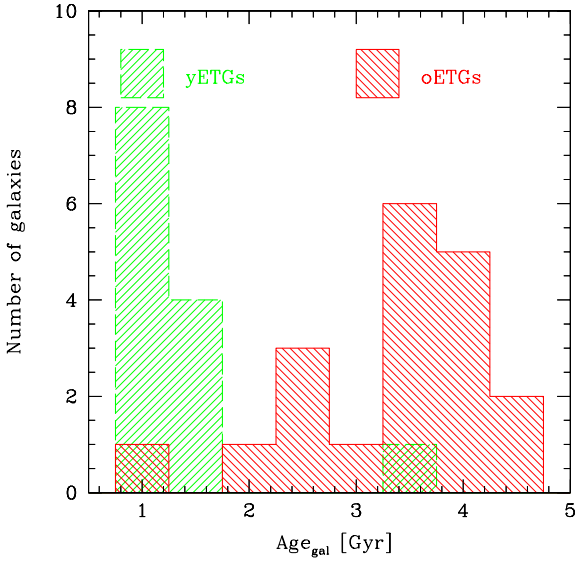

Figure 5. Age distributions of the two sub-sample of ETGs. The dashed (green) histogram represents the distribution of the 13 ETGs whose SB agrees with the local KR in case of luminosity evolution. The solid (red) histogram represents the distribution of the remaining 19 ETGs whose SB exceeds by more than one σ the KR.

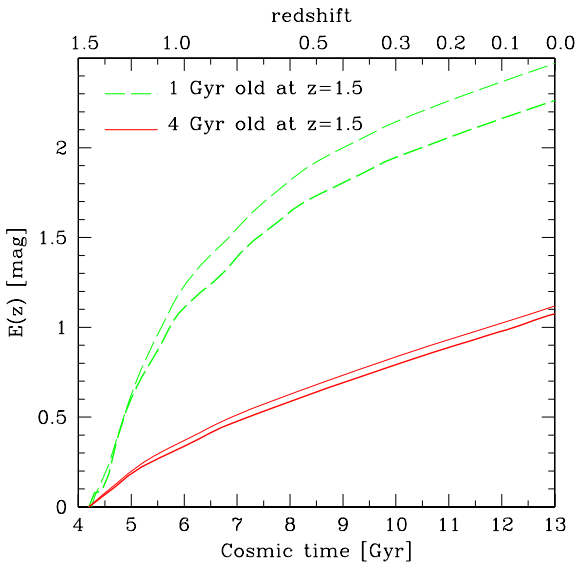

Figure 6. Evolution term $E(z)$ as a function of the cosmic time (bottom x-axis) or redshift (upper x-axis) for two galaxies which at $z = 1.5$ are 1 Gyr old (dashed green line) and 4 Gyr old (solid red lines), respectively. The thin lines have been obtained with a SFH described by $\tau = 0.1$ Gyr and the thick lines refer to a model with $\tau = 0.3$ Gyr.

respect to the KR. Fig. 6 displays the evolution term $E(z)$ in the R band as a function of the cosmic time (bottom x-axis) or redshift (upper x-axis) for two galaxies whose stellar populations at $z = 1.5$ are 1 Gyr old (dashed red line) and 4 Gyr old (solid red line). The thin lines refer to a SFH with $\tau = 0.1$ Gyr while the thick lines refer to $\tau = 0.3$ Gyr. In fact, we see that the difference in the luminosity evolution $E(z)$ between the old and the young stellar population is about 1 mag at $z = 0$ independently of the different values of τ. Thus, the different mean age of the stellar populations of ETGs at $z \sim 1.5$ is the reason of their different expected evolution. We have also compared the absolute magnitude distribution and the stellar mass distribution of these two populations to gather other information about their evolutionary status and to search for signs of different history of star formation and mass assembly. In Fig. 7, we show the distributions of the absolute magnitude (left-hand panel) and of the stellar mass (right-hand panel) of the yETGs (dashed red histogram) and of the oETGs (solid red histogram). We see that yETGs tend to be less luminous and, accordingly, less massive than the oETGs even if the effect is not statistically significant, as confirmed by the KS test performed to compare the two distributions [$P(D > D_{max}) = 0.02$]. However, it can be seen that the high-luminosity/mass tail is populated only by old ETGs while the low-luminosity/mass tail is composed of only young ETGs.

The SED fitting of our ETGs is based on optical and near-IR photometry which at $z \sim 1.5$ samples the wavelength range $\lambda < 0.8\,\mu$m. In practice, at this redshift, six out of the eight to nine photometric points sample the UV and blue rest-frame emission of the galaxies whose continuum shape is affected by star formation episodes even if involving a negligible fraction of the stellar mass (see e.g. fig. 2 in Longhetti et al. 2008). For this reason, it is more appropriated to consider the age we derived as a lower limit to the time elapsed since the last episode of star formation. If this latter is the major one, then this age will provide the formation redshift of the stellar population. Given the different age of the two populations of ETGs, it is likely that the formation redshift of their stellar populations is different. In particular, the stellar component of the oETGs ($Age_{med} \sim 3.5$) formed at $z_f \sim 5$–6 while the stellar populations of yETGs ($Age_{med} \sim 1$) formed at $z_f > 2.5$–3, or at least the youngest population.

6 THE SIZE-LUMINOSITY AND THE SIZE-MASS RELATIONS

The dependence of the characteristic size of galaxies on their luminosity and on their stellar mass has been recently studied for large samples of local galaxies (e.g. Shen et al. 2003), at intermediate redshift ($z \sim 1$; McIntosh et al. 2005) and at high redshift ($z < 3$) (e.g. Trujillo et al. 2004, 2006b; Cimatti et al. 2008; van Dokkum et al. 2008). Shen et al. (2003) on the basis of the Sloan Digital Sky Survey (SDSS) data show that the size of local early types and late types increases, as expected, according to their luminosity and stellar mass. However, the ETGs follow steeper relations than late types showing that the size of a stellar system is not simply a function of its mass and that the history of its mass assembly can affect these relations (Shen et al. 2003). McIntosh et al. (2005) study the evolution of these relations up to $z < 0.8$–1 by combining GEMS data (Galaxy Evolution from Morphology and SEDs; Rix et al. 2004) with COMBO-17 data (Classifying Objects by Medium-Band Observations; Wolf et al. 2003) while Trujillo et al. (2007) extend the study up to $z \sim 2$, thanks to the DEEP-2 survey (Davis et al. 2003; Bundy et al. 2006) and to $z \sim 3$ (Trujillo et al. 2004), thanks to the FIRES data (Franx et al. 2000). Our data allow us to define these relations for a sample of ETGs at $1 < z < 2$ with secure spectroscopic redshift and classification and on the basis of the morphology derived by their red rest-frame continuum.

The size-luminosity (SL) relation for our sample at $z \sim 1.5$ is shown in Fig. 8 (left-hand panel) and it is compared with the relation found in the r band by Shen et al. (2003) using the Sérsic half-light radius for local ETGs (solid line)

$$\log(R_e) = -0.26 M_R - 5.06. \quad (9)$$

The dotted lines represent the scatter of the relation. Young ETGs are marked with (green) squares while old ETGs with (red) points.

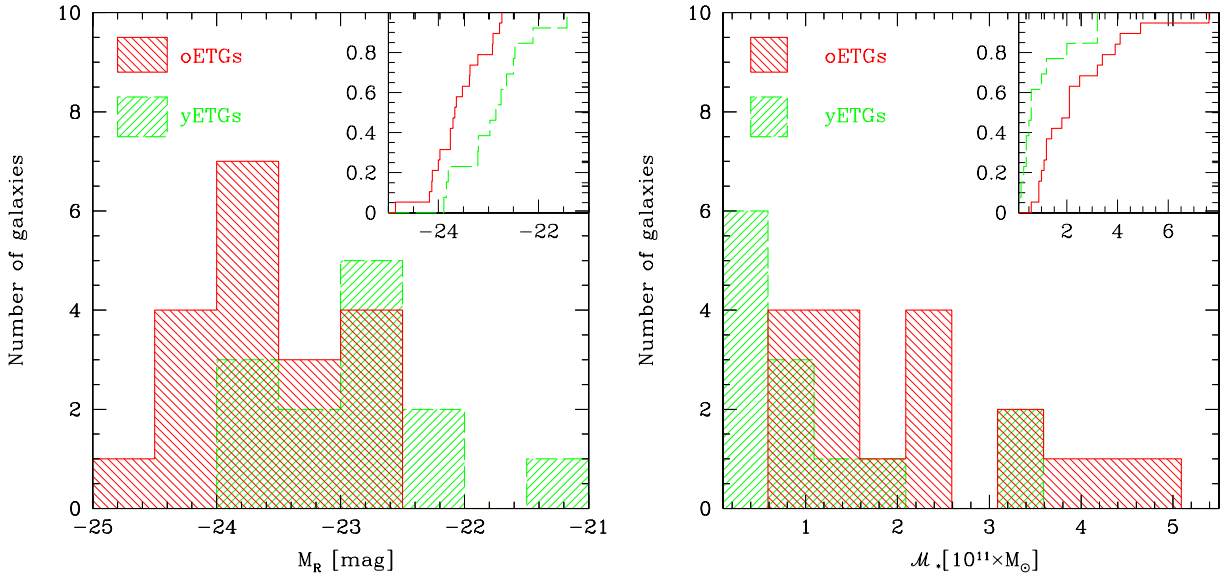

Figure 7. Distribution of the R-band absolute magnitude M_R (left-hand panel) and of the stellar mass $\mathcal{M}_*$ for the 13 yETGs (dashed green histogram) and for the 19 oETGs (solid red histogram). The inside panels show cumulative distributions. The KS test performed provides a probability that the two distributions come from the same population $P \simeq 0.02$.

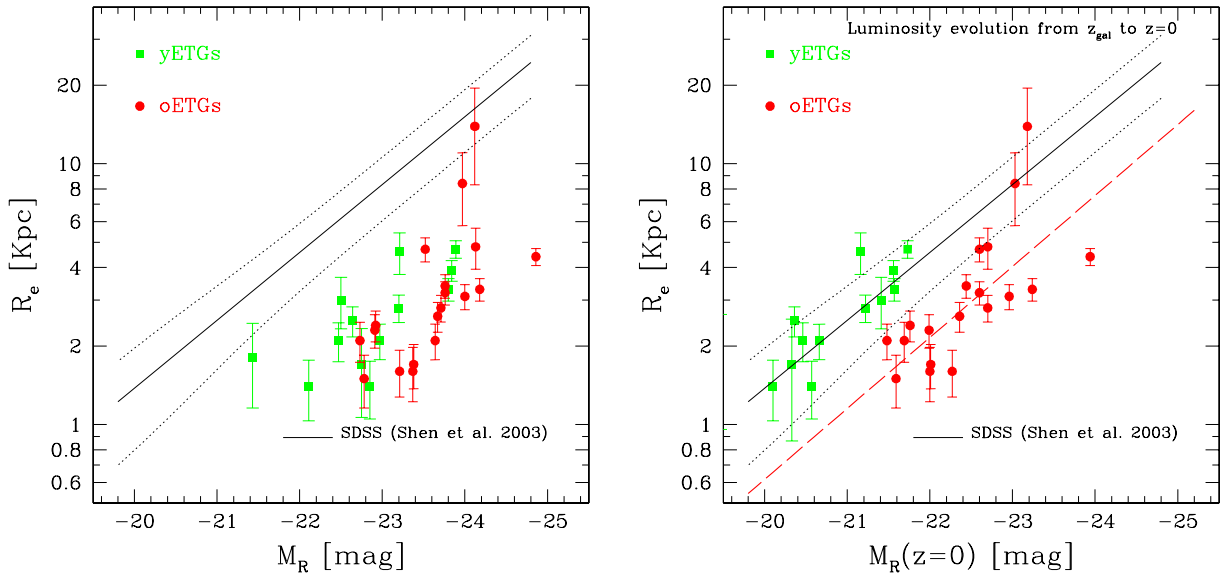

Figure 8. Left-hand panel: SL relation for our sample of yETGs (green squares) and oETGs (red points) at $z \sim 1.5$ compared with the local relation found by Shen et al. (2003, solid line). The dotted lines represent the scatter of the relation. Right-hand panel: SL relation in the case of pure luminosity evolution. It is shown how the 32 ETGs of our sample would be displaced at $z = 0$ in the (R_e, M_R) plane in case of pure luminosity evolution, i.e. the R-band absolute magnitude plotted is $M_R(z = 0) = M_R(z) - E(z)$. The dashed (red) line is the best-fitting relation $\log R_e = -0.28 M_R(z = 0) - 5.6$ to the oETGs (see Section 6).

The R-band absolute magnitude M_R of our galaxies is the one at the redshift of the galaxies. The offset with respect to the relation of Shen et al. reflects the evolution which ETGs undergo from their redshift to $z = 0$, the same evolution observed in the comparison of the KR shown in Fig. 4 (the one at $z \sim 1.5$ and the other at $z = 0$). It is worth noting that the difference between the r photometric band of the SDSS and the R Cousins band we use is about 0.2 mag (Fukugita, Shimasaku & Ichikawa 1995). Thus, the possible uncertainties related to the transformation between the two filters are negligible.

In the right-hand panel of Fig. 8, we show how the 32 ETGs of our sample would be displaced at $z = 0$ in the (M_R, R_e) plane in case of pure luminosity evolution, i.e. the R-band absolute magnitude plotted is $M_R(z = 0) = M_R(z) - E(z)$. In this case, the different behaviour shown by the young ETGs with respect to the old ETGs is even sharper than in the case of the KR (Fig. 4). It is evident the agreement between the young ETGs and the local SL relation once considered their own luminosity evolution. All the yETGs are located within the scatter region of the $z \sim 0$ relation. On the contrary, it is evident the disagreement between the old ETGs and

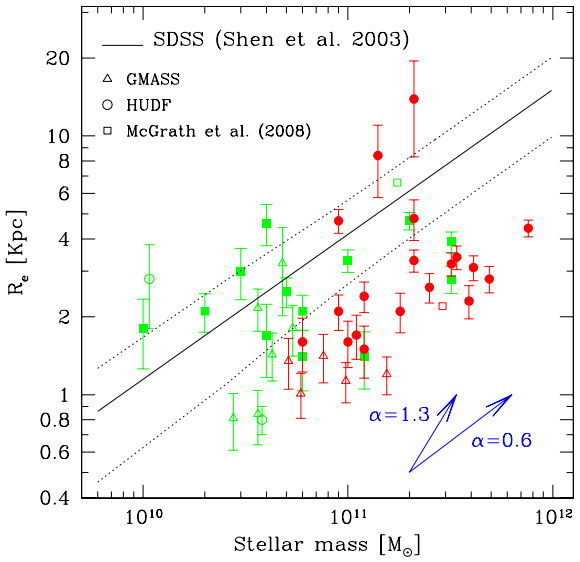

Figure 9. SM relation for our sample of ETGs (filled symbols) compared with the local relation found by Shen et al. (2003, solid line). The dotted lines represent the scatter of the relation. Red symbols mark the oETGs while green symbols mark the yETGs The two vectors represent the relation found by BK06 for the two extreme values $\alpha = 0.6$ and 1.3. The open symbols (triangles, circles, squares) indicate the galaxies of the GMASS sample (Cimatti et al. 2008), the two passive galaxies in the HUDF from Daddi et al. (2005) and the two spheroids of McGrath et al. (2008). We classified as old (and consequently marked with red colour) those galaxies older than 2.0 Gyr.

the local SL relation, disagreement which shows clearly that R_e must change from $z \sim 1.5$ to $z \simeq 0$. It is worth noting that the calibration of the SL relation based only on the oETGs data is

$$\log(R_e) = -0.28 M_R(z = 0) - 5.6$$

[dashed (red) line in Fig. 8], a relation with the same slop of the one at $z \sim 0$ but with an offset of $\sim$0.5 in the zero-point corresponding to a factor of $\sim$3 in R_e.

In Fig. 9, our galaxies (filled symbols) are plotted on the size-mass (SM) plane and compared with the SM relation found by Shen et al. (2003) for the local ETGs (solid line) expressed by the following equation:

$$R_e = 2.88 \times 10^{-6} (\mathcal{M}_*/\mathcal{M}_\odot)^{0.56}. \quad (10)$$

The stellar mass they use is the one from Kauffmann et al. (2003) based on the Bruzual & Charlot (2003, hereafter BC03) models and on the Kroupa (2001) IMF while we used the CB08 models and Chabrier IMF. Longhetti et al. (2008) show that the stellar mass obtained with Kroupa IMF differs by less than 5 per cent from the one obtained with Chabrier IMF and that the use of BC03 models leads to overpredict the mass estimate by a factor of 1.2–1.3 with respect to CB08 models. Thus, we decided not to apply any scaling factor to the relation found by Shen et al. (2003) given such small differences. Fig. 9 shows that while nine out of the 13 yETGs (70 per cent) follow this SM relation at $z \sim 0$, only four out of the 19 oETGs (20 per cent) agree with this relation. The yETGs for which the luminosity evolution is requested to bring them on the local SL relation do not need any mass or size evolution since they naturally match the local SM relation. In other words, this is an evidence that yETGs are fully compatible with a simple evolution from $z \sim 1.5$–2 to $z = 0$ of their $\mathcal{M}/L$ ratio due to pure luminosity evolution while their stellar mass remains unchanged. On the contrary, the old ETGs follow well-defined SL and SM relations but almost all of them have sizes much smaller than at $z \sim 0$ implying that they have changed significantly their structure from $z \sim$ 1.5–2 to $z = 0$. Using the relation of Shen et al. (eq. 10), we have derived the mean value $\langle f_{R_e} \rangle = 1/N \sum(R_{e,0}/R_{e,z})$, i.e. the ratio between the radius R_e of the 15 oETGs which do not follow the local SM relation and the radius of the local ETGs with similar mass. We have obtained $\langle f_{R_e} \rangle = 2.6 \pm 0.5$ in agreement with the value 3.4 ± 1.7 found by Cimatti et al. (2008) in the same redshift range.} Thus, the oETGs must increase their size by a factor of 2.6 from $z \sim 1.5$ to 0, consistently with the result obtained from the KR and the SL relation. It is worth noting that even hypothesizing that we have systematically overestimated by a factor of 2 the mass of all the oETGs their effective radius would be still 1.7 times larger than locally, i.e. they would be five times denser. To move the oETGs on to the local SM relation, their stellar mass should be six times smaller, a factor too large to be accounted for by any model assumption. In Fig. 9, a collection of ETGs at $1.3 < z < 2$ (open symbols) taken from the literature is also shown. Triangles, circles and squares mark the GMASS galaxies from Cimatti et al. (2008), the two HUDF galaxies from Daddi et al. (2005) and the two spheroids of McGrath et al. (2008), respectively. The redshift and the spectral type of these ETGs are spectroscopically confirmed and the morphology is based on *HST*-ACS (advanced camera for surveys) observations. According to the analysis performed by the authors and to the parameters they derived, we divided this sample of ETGs in old and young, defining the old as those ETGs with age larger than 2 Gyr. The old ETGs are marked by red open symbols while the young ETGs are marked by green open symbols. It is remarkable the agreement with the behaviour shown by our sample of 32 galaxies: young ETGs tend to distribute according to the local SM relation (six out of nine) while none of the old ETGs follows the local SM relation.

It should be noted, however, that a non-negligible fraction of yETGs, both in our sample of 32 ETGs and in the sample taken from the literature, does not follow the SM relation but follows the relation defined by the old ETGs. Thus, for some yETGs a major size evolution is still required. If this result will be confirmed on a more solid statistical ground proving that it is not due to an internal scatter in the estimate of the physical parameters (age, stellar mass and effective radius), it implies that yETGs follow different histories of assembly and are less homogeneous than old ETGs. We will try to constrain their evolutionary path in the next section.

7 CONSTRAINING THE FORMATION AND THE EVOLUTION OF ETGs

The analysis performed in the previous sections shows that two populations of ETGs exist at $z \sim 1.0$–2.0. They differ substantially for the age of their stellar populations by about 2 Gyr and for the scaling relations they follow. It is natural to ask how these two populations evolved from $z \lesssim 2$ to $\sim$0 to match the properties of the local ETGs and which is their assembly history they followed to have the properties shown at $z \sim 1.5$. We have tried to answer these questions placing our results in the hierarchical paradigm of galaxy formation and evolution taking into account the results obtained from various renditions of merging models.

7.1 Tracing the evolution at $z \lesssim 2$

The older ETGs of our sample at $z \simeq 1.5$–2 do not follow the SM relation of local ETGs as well as the other scaling relations. Pure

luminosity evolution from their redshift to $z = 0$ does not bring them on to the local KR and SL relation. oETGs are characterized by effective radii $R_e \sim 2.5$–3 times smaller than those of the local ETGs with comparable SB, absolute magnitude and stellar mass as deduced from the comparison with the local KR and SL and SM relations. Thus, an evolution of their size between $z \sim 1.5$–2 and $z = 0$ must occur to bring them on to the local scaling relations. Such size evolution is often used to advocate the merging processes the ETGs should experience during their life in the hierarchical paradigm of galaxy formation and evolution (e.g. Trujillo et al. 2004, 2007; Bell et al. 2006; De Lucia et al. 2006; van Dokkum et al. 2008; van der Wel et al. 2008). Merging is indeed usually invoked as the most obvious and efficient mechanism to increase the size of galaxies.

Boylan-Kolchin, Ma & Quataert (2006, hereafter BK06), using simulations of dissipation-less merging, the so-called 'dry merging' (e.g. van Dokkum 2005; Bell et al. 2006 and references therein), show that the remnants of dry mergers lie on the fundamental plane (FP; Djorgovsky & Davis 1987; Dressler et al. 1987) of their progenitors. However, the locations of the remnants in the projections of the FP, in particular on the R_e–$\mathcal{M}_*$ relation, depend strongly on the merger orbit. Thus, the projections of the FP can provide a tool to investigate the assembly history of ETGs. In their analysis, they find that the expected increase of the size of an ETG due to merging follows the relation $R_e \propto \mathcal{M}_*^{\alpha}$ with $0.6 < \alpha < 1.3$ (represented by vectors in Fig. 9) depending on the orbital properties (see also Nipoti, Londrillo & Ciotti 2002; Ciotti, Lanzoni & Volonteri 2007). They also show that the index α is almost independent of the mass ratio of the progenitors (see also Khochfar & Silk 2006a for a similar result) suggesting that their findings are applicable both to minor and to major mergers. We have tried to consider this model of dry merging to increase the size of oETGs. We have seen that the effective radii of oETGs must increase by a factor $\langle f_{R_e} \rangle \simeq 2.6$ from $z \sim 1.5$ to 0 in order to match the local SM relation. Thus, the condition $R_f \simeq 2.6 R_i$ where R_i and R_f are the radii before (initial) and after (final) the merging must be satisfied. From the relation of BK06, it follows that $\mathcal{M}_f^{\alpha} \simeq 2.6 \mathcal{M}_i^{\alpha}$ where $\mathcal{M}_i$ and $\mathcal{M}_f$ are the masses before and after the merging. Consequently, the mass $\mathcal{M}_f$ that the remnant must reach to increase the size 2.6 times is

$$\mathcal{M}_f = 2.6^{1/\alpha} \mathcal{M}_i. \tag{11}$$

The most efficient way to move oETGs from their location on to the local SM relation is for $\alpha = 1.3$ (see vectors in Fig. 9), the maximum value found by BK06 which, by the way, minimizes the stellar mass of the remnant. We thus obtain

$$\mathcal{M}_f \geq 2.1 \mathcal{M}_i, \qquad \alpha \leq 1.3, \tag{12}$$

i.e. the mass of the remnant is at least twice the mass before the merging. Any value of α lower than 1.3 would produce larger masses. This result is difficult to reconcile with the number density of high-mass ETGs in the local universe. Indeed, this mechanism would produce too much ETGs with masses much larger than $10^{11}\,M_\odot$ and an evolution in the stellar mass density at $z < 2$ which is not observed (see e.g. Conselice et al. 2007). For instance, Saracco et al. (2005) show that the seven galaxies, S2F1# also studied in the present paper, account for 70 per cent of the local population of ETGs with comparable luminosity and mass. If they twice their mass/luminosity, at $z \sim 0$ we should observe two to three times more ETGs with masses $\mathcal{M}_* \geq 4 - 5 \times 10^{11}\,M_\odot$ than those in fact observed. Moreover, as noted previously by Cimatti et al. (2008), it is difficult to imagine that given all possible orbital parameters in merging events, the effective value of α is always close to the maximum one. Finally, we recall that values $\alpha < 1.3$ would worsen the disagreement with the local number of high-mass ETGs. Thus, we conclude that merging cannot be the mechanism with which oETGs increase their size at $z < 2$ and that it is not the way to solve the problem. Other mechanisms able to increase the size but to leave nearly unchanged the mass of ETGs must occur. Close encounters or, more generally, interactions between galaxies can act in this way. Their frequency and thus their efficiency depend on the number of close encounters that a galaxy can experience in the last 9–10 Gyr of its life, a number that perhaps can be constrained from the statistics of pairs and from simulations. Minor or 'satellite' merging (e.g. Naab et al. 2007), i.e. merging between galaxies with masses $\mathcal{M}_1$ and $\mathcal{M}_2$ in the ratio ~0.1:1 or lower, would produce remnants with masses of the order of $\mathcal{M}_2$ but with larger size. The ability of this kind of merging in enlarging the size is not clear; however it could act in the right way contributing to solve the problem of the small sizes of oETGs.

The younger population of ETGs, the yETGs, follows the SM relation of local ETGs, with few exceptions. Luminosity evolution from $z \sim 1.5$–2 to $z = 0$, i.e. for fixed size R_e, would bring the yETGs on to the local KR and SL relation. Thus, for these galaxies, the evolution of the $\mathcal{M}/L$ ratio due to the expected luminosity evolution explains their observed properties at $z \sim 1.5$–2 and brings them to agree with the scaling relations of local ETGs. This suggests that the buildup of yETGs was already completed at $z \sim 2$ providing no evidence in favour of merging at $z < 2$ since it would bring them out of the SM relation and the other scaling relations. Indeed, merging, to move yETGs along the SM relation, should take place for values $\alpha \simeq 0.6$ (see vectors in Fig. 9) producing remnants with masses $\mathcal{M}_f \sim 5 \mathcal{M}_i$. For the analogous reasons discussed above, it is difficult to imagine that given all possible orbital parameters in merging events, the effective value of α for yETGs is always close to the minimum one. Moreover, the luminosity at $z \sim 0$ of the remnant should dim according to the increased size in order to match the KR and the SL relation. These requirements and fine-tuning make this picture rather unlikely. Finally, the reasoning relevant to the exceeding number of remnant ETGs with masses well in excess of $10^{11}\,M_\odot$ applies also in this case, and corroborates the conclusion that the assembly of yETGs was completed at $z \sim 2$ and that no merging has happened at $z < 2$. We cannot rule out that yETGs may experience satellite merging at $z < 2$ if it leaves nearly unchanged their size besides their stellar mass.

For the reasons discussed here, we can conclude that ETGs, both young and old, have already reached their final stellar mass at $z \lesssim 2$. Major merging at redshift $z < 2$, if any, must necessarily involve a negligible fraction of the old ETGs while satellite merging could involve both yETGs and oETGs even if in a different way.

7.2 Constraining the path at $z > 2$: toward the formation of ETGs

The older ETGs are characterized by a median age of about 3.5 Gyr (and a dispersion of about 1 Gyr) which implies that their stars formed at $z_f \sim 5$–6. Given the short time they have at disposal to form masses of the order of $10^{11}\,M_\odot$ of stars the SFR was necessarily SFR $> 100\,M_\odot\,\mathrm{yr}^{-1}$ (see also Cimatti et al. 2004, 2008; McCarthy et al. 2004; Daddi et al. 2005; Longhetti et al. 2005; Feulner et al. 2005; Kriek et al. 2006). Moreover, oETGs are 2.5–3 times smaller than those at $z \sim 0$, thus the physical mechanism(s) acting at $z > 2$ must be capable also to produce very compact galaxies with stellar densities 15–30 times higher than the local ones and than the yETGs. Dissipational gas-rich merging can produce highly compact massive ETGs if a high fraction of stars of the remnant

formed during the merger in a violent starburst (e.g. Springel & Hernquist 2005; Khochfar & Silk 2006a). However, it is not clear whether the typical time-scale of major merging can fit with the above requirements ($\tau_{\rm merge} > 3$ Gyr from Boylan-Kolchin, Ma & Quataert 2008). Naab et al. (2007), with their *ab initio* hydrodynamic simulations, show that the early formation phase of galaxies can start with an initial burst of star formation at $z \sim 5$ accompanied by mergers of gas-rich small sub-components and *in situ* intense star formation. Although some fraction of the stars is accreted (the 'quiescent' component; Khochfar & Silk 2006b), Naab et al. show that this phase has the characteristics of a dissipative collapse since it happens on very short time-scale. Thus, the compactness of ETGs produced through the gas-rich merging of Kochfar et al. (2006) and the rapid dissipative collapse of Naab et al. (2007) provides a scenario which seems to fit, at least qualitatively, the intense SFR required at $z \sim 5$–6 and the need to assemble ETGs which at $z \lesssim 2$ are compact and old.

The younger population, the yETGs, is characterized by a median age of ∼1 Gyr and a dispersion of about 0.2 Gyr, which push the last burst of star formation at $z_{\rm f} > 2.5$. In this case, the constraints on the possible physical mechanism(s) acting at $z > 2$ are less stringent than those required to assemble oETGs at the same redshift. A scenario in which yETGs accreted stellar mass by subsequent episodes of merging and by star formation *in situ* (which can also be triggered by satellite and secondary merging events) can qualitatively fit the properties of these yETGs which at $z < 2$ must appear younger and already enlarged in their size if compared with the local ones. The few of them which appear much more compact than the other yETGs could be the result of the gas-rich merging scenario proposed by Kochfar et al. (2006) and Naab et al. (2007) characterized by a rapid dissipative collapse that happened at $z \gtrsim 2.5$.

From the observational point of view, the two populations of ETGs should have different progenitors. oETGs must experience a phase of intense star formation at high z ($z \gtrsim 5$), while yETGs can experience this phase at lower redshift or experience subsequent episodes of star formation possibly triggered by satellite merging. In any case, a different epoch of formation and assembly must characterize the two populations of ETGs. This result qualitatively agrees with the model of Khochfar & Silk (2006a), which indicates that the scatter in the size of similar present-day ellipticals is a result of their formation epoch, with smaller ellipticals formed earlier through mergers much richer of gas than the mergers assembling larger ellipticals. In Fig. 10, the predicted evolution of sizes for ETGs with respect to the sizes of their local counterparts from the model of Khochfar & Silk (2006a) is compared to the observed ratio $R_{\rm e}(z)/R_{\rm e}(z=0)$ for our sample of 32 ETGs. This ratio has been obtained for each galaxy dividing the observed effective radius by that derived by the SM relation of Shen et al. (2003) for the same mass of the galaxy. As expected, oETGs are preferentially located on the curve representing the largest ratio which is expected for the highest-mass ETGs since they should form much earlier in the model. On the contrary yETG are preferentially located on to or even above the curves representing the minimum size evolution which is expected for the lower mass ETGs which should form later. It is worth noting that while this model reproduces very well the observed relation between size evolution and formation epoch of ETGs (the older the more compact/denser), the correlation with the stellar mass is less evident from our data and a larger sample would be needed to probe this issue. As to the progenitor candidates, as suggested by Cimatti et al. (2008), a possible population of progenitors could be the sub-mm-selected galaxies seen at $z \gtrsim 3$ (e.g. Blain et al. 2002; Tacconi et al. 2006; Tacconi, Genzel & Smail 2008) whose characteristics could fit those of ETGs at $1 < z < 2$. Even if it is difficult to identify the progenitors, we can try to constrain their redshift. Given the properties of oETGs (old and compact at $z \lesssim 2$) and the typical time-scale of merging ($\tau_{\rm merge} > 3$ Gyr), we should expect to see oETGs till $z \sim 3$–3.5, the only difference should be the age of their stellar population correspondingly younger. On the contrary, yETGs should appear quite different at $z > 2.5$, most probably in the phase of merging, or star forming and interacting with other galaxies.

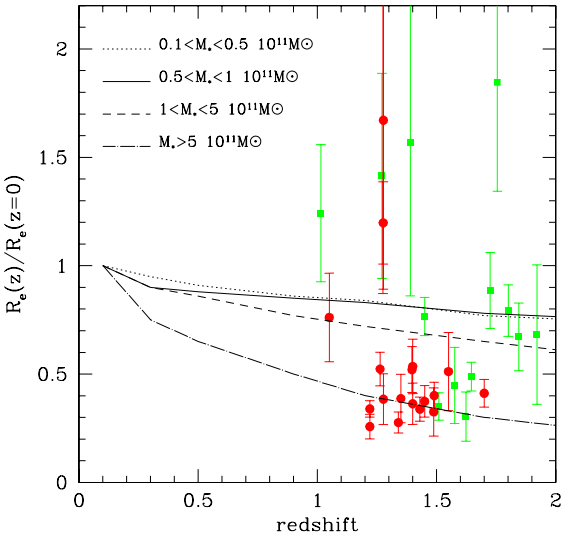

Figure 10. The ratio $R_{\rm e}(z)/R_{\rm e}(z=0)$ (filled symbols) obtained dividing the observed effective radius of our galaxies by that derived by the SM relation at $z = 0$ of Shen et al. (2003) for the same mass is compared to the predicted evolution of sizes (curves) from the model of Khochfar & Silk (2006a). Symbols are as in Fig. 8. Dotted, solid, dashed and dot–dashed curves represent the predictions for the different ranges of stellar masses listed in the legend.

8 SUMMARY AND CONCLUSIONS

We presented the morphological analysis of a sample of 32 ETGs at $1 < z < 2$ with spectroscopic confirmation of their redshift and spectral type based on *HST*-NICMOS observations in the F160W filter. These 32 ETGs have been selected from different samples and surveys on the basis of their spectroscopic and morphological classification and are characterized by a multiwavelength coverage. The *HST*-NICMOS observations in the F160W filter have allowed us to derive the effective radius $R_{\rm e}$ and the mean SB $\langle\mu\rangle_{\rm e}$ of galaxies in the rest-frame *R* band of the galaxies, less affected by morphological *k*-correction and star formation than the optical bands usually used in the previous works. Through the best fitting of their SEDs at known redshift, we derived the *R*-band absolute magnitude, the stellar mass and the age for each of them. The main results of the analysis we performed can be summarized as follows.

(i) The 32 ETGs of our sample at $1 < z < 2$ are placed on the ($\langle\mu\rangle_{\rm e}$, $R_{\rm e}$) plane defining a relation with the same slope of the KR at $z \sim 0$ but with a different zero-point which accounts for the evolution they undergo from $z \simeq 1.5$–2 to $z = 0$. We do not see differences between the six ETGs in clusters and the other ETGs in agreement with other works (e.g. Gobat et al. 2008; Rettura et al. 2008) even if the very low statistics we have do not allow us a detailed comparison of different environments.

(ii) The ETGs of our sample are composed of two distinct populations which differ for the age of their stellar populations: the older population, the oETGs, has a median age of about 3.5 Gyr which implies that the bulk of stars formed at $z_f \sim 5$–6; the younger population, the yETGs, has a median age of about 1 Gyr and correspondingly $z_f > 2.5$–3. Even if the absolute values of these ages can be model dependent, the different age cannot be accounted for by any model assumption while it is reliable an age difference of about 1.5–2 Gyr for the two populations of ETGs. yETGs tend to be less luminous and correspondingly less massive than oETGs even if this tendency is more evident in the tails of the distributions.

(iii) yETGs follow the SM relation locally observed (Shen et al. 2003), and their expected luminosity evolution from $z \sim 1.5$–2 to $z = 0$ at fixed size R_e brings them on to the local KR and SL relation. Thus, their SB and stellar mass density do not exceed those of local ETGs with comparable luminosity and stellar mass, i.e. no size evolution is required at $z < 2$. These properties suggest that young ETGs have already completed the growth of their stellar mass at $z \sim 2$ being on to the SM relation and that they must evolve at $z < 2$ purely in luminosity to match the local KR and SL relation. This provides no evidence in favour of major merging at $z < 2$ since it would bring them out of the local scaling relations.

(iv) oETGs do not follow the local SM relation since they have sizes 2.5 to three times smaller than those provided by the SM relation at their stellar masses. Pure luminosity evolution from their redshift to $z \sim 0$ is not sufficient to bring them on to the local KR and SL relation. Also, in this case the effective radii are 2.5–3 times smaller than the local ETGs with comparable SB and absolute magnitude. Thus, an evolution of their size at $z < 2$ must occur to reconcile the oETGs with the local population of ETGs. Major (dry) merging at $z < 2$ cannot solve the problem since it would produce too much ETGs with stellar masses $>5 \times 10^{11}$–10^{12} $M_\odot$, and it should happen only under particular orbit conditions to move oETGs on to the local SM relation. Other mechanisms able to increase the size and to keep constant the stellar mass of oETGs (e.g. satellite merging, close encounters) must be invoked.

(v) The different properties shown by the yETGs and the oETGs at $1 < z < 2$ imply different evolutionary paths from their formation to $z \lesssim 2$. oETGs are much more compact and hence denser than local ones (15–30 times denser than both the local ETGs with comparable stellar mass and yETGs); they are old with respect to the age of the universe at their redshift. Thus, their stellar mass must have formed at high redshift ($z \sim 5$) following a sort of dissipative gas-rich collapse able to form rapidly most of the stellar mass, thus producing a compact old remnant at $z \lesssim 2$. This scenario is qualitatively fitted by the merging models of Khochfar et al. (2006) and Naab et al. (2007). Considering the typical time-scale of merging ($\tau_{merge} > 3$ Gyr; Boylan-Kolchin et al. 2008) and the age of the stellar population of oETGs, we conclude that oETGs must exist as they are till $z \gtrsim 3$–3.5 with stellar populations correspondingly younger. Progenitors should be searched for among the population of galaxies at $z > 3.5$–4 as high-mass galaxies with intense star formation. Possible candidates could be the sub-mm/selected galaxies (e.g. Blain et al. 2002; Tacconi et al. 2006, 2008) as suggested by Cimatti et al. (2008).

The formation scenario for the yETGs seems to be rather different even if less constrained with respect to the one of the oETGs. The age of the yETGs implies that the last burst of star formation has taken place close to their redshift, i.e. $z \sim 2.5$. They are not denser than the local one and are placed on the local SM relation. They have completed their stellar mass growth as the oETGs but in a way such that their size is larger. Major merging, satellite merging and close encounters coupled with star formation *in situ* can qualitatively fit these requirements producing at $z \lesssim 2$ ETGs with a young component of the stellar population and sizes comparable to those of the local ETGs with similar stellar mass, SB and luminosity. This population of yETGs should appear at $z > 2.5$–3 as star-forming and/or interacting galaxies.

On the basis of the above results, we believe that a key observational test would be the measure of the velocity dispersion of oETGs and yETGs since such quantity would unambiguously address the question whether the two populations are dynamically different, thus providing unique constraints on the mechanism of their formation and on their size evolution at $z < 2$.

ACKNOWLEDGMENTS

Based on observations made with the NASA/ESA *HST*, obtained at the Space Telescope Science Institute, which is operated by the Association of Universities for Research in Astronomy, Inc., under NASA contract NAS 5-26555. This work has received partial financial support from the Istituto Nazionale di Astrofisica (Prin-INAF CRA2006 1.06.08.04) and from ASI (contract I/016/07/0).

REFERENCES

Abraham R. G. et al., 2004, AJ, 127, 2455
Arnouts S. et al., 2007, A&A, 476, 137
Bell E. F. et al., 2006, ApJ, 640, 241
Bertin E., Arnouts S., 1996, A&AS, 117, 393
Blain A., Smail I., Ivison R. J., Kneib J.-P., Frayer D. T., 2002, Phys. Rep., 369, 111
Bolzonella M., Miralles J.-M., Pellò R., 2000, A&A, 363, 476
Boylan-Kolchin M., Ma C.-P., Quataert E., 2006, MNRAS, 369, 1089 (BK06)
Boylan-Kolchin M., Ma C.-P., Quataert E., 2008, MNRAS, 383, 93
Bruzual A. G., Charlot S., 2003, MNRAS, 344, 1000 (BC03)
Buitrago F., Trujillo I., Conselice C. J., Bouwens R. J., Dickinson M., Yan H. 2008, ApJ, 687, L61
Bundy K. et al., 2006, ApJ, 651, 120
Calzetti D., Armus L., Bohlin R. C., Kinney A. L., Koorneef J., Storchi-Bergmann T., 2000, ApJ, 533, 682
Caputi K. I. et al., 2007, ApJ, 660, 97
Cassata P. et al., 2005, MNRAS, 357, 903
Chabrier G., 2003, PASP, 115, 763
Chen H.-W. et al., 2002, ApJ, 570, 54
Cimatti A. et al., 2002, A&A, 392, 395
Cimatti A. et al., 2004, Nat, 430, 184
Cimatti A., Daddi E., Renzini A., 2006, A&A, 453, L29
Cimatti A. et al., 2008, A&A, 482, 21
Ciotti L., Lanzoni B., Volonteri M., 2007, ApJ, 658, 65
Cirasuolo M. et al., 2007, MNRAS, 380, 585
Cirasuolo M. et al., 2008, MNRAS, submitted (arXiv:0805.1335)
Coe M. J., Benítez M., Sánchez S. F., Jee M., Bouwens R., Ford H., 2006, AJ, 132, 926
Conselice C. J. et al., 2007, MNRAS, 381, 962
Daddi E. et al., 2005, ApJ, 626, 680
Damjanov I. et al., 2008, ApJ (arXiv:0807.1744v2)
Davis M. et al., 2003, proc. SPIE, 4834, 161
De Lucia G., Springel V., White S. D. M., Croton D., Kauffmann G., 2006, MNRAS, 366, 499
de Vaucouleurs G., 1948, Ann. d'Astrophys., 11, 247
di Serego Alighieri S. et al., 2005, A&A, 442, 125
Djorgovsky S., Davis M., 1987, ApJ, 313, 59
Dressler A., Lynden-Bell D., Burstein D., Davies R. L., Faber S. M., Terlevich R., Wegner G., 1987, ApJ, 313, 42
Drory N. et al., 2001, MNRAS, 325, 550

Drory N., Salvato M., Gabasch A., Bender R., Hopp U., Feulner G., Pannella M., 2005, ApJ, 619, L131
Dunlop J., Peacock J., Spinrad H., Dey A., Jimenez R., Stern D., Windhorst R., 1996, Nat, 381, 581
Farrah D. et al., 2006, ApJ, 641, L17
Feulner G., Gabasch A., Salvato M., Drory N., Hopp U., Bender R., 2005, ApJ, 633, L9
Feulner G., Goranova Y., Hoop U., Gabasch A., Bender R., Botzler C. S., Drory N., 2007, MNRAS, 378, 429
Firth A. et al., 2002, MNRAS, 332, 617
Fontana A. et al., 2004, A&A, 424, 23
Franx M. et al., 2000, The Messenger, 99, 20
Fukugita M., Shimasaku K., Ichikawa T., 1995, PASP, 107, 945
Glazebrook K. et al., 2004, Nat, 430, 181
Gobat R., Rosati P., Strazzullo V., Rettura A., Demarco R., Nonino H., 2008, A&A, 488, 853
Kauffmann G. et al., 2003, MNRAS, 341, 33
Khochfar S., Silk J., 2006a, ApJ, 648, L21
Khochfar S., Silk J., 2006b, MNRAS, 370, 702
Kong X. et al., 2006, ApJ, 638, 72
Kormendy J., 1977, ApJ, 218, 333
Kriek M. et al., 2006, ApJ, 649, L71
Krist J., 1995, in Shaw H. E., Payne H. E., Hayes J. J. E., eds, ASP Conf. Ser. Vol. 77, Astronomical Data Analysis Software and Systems IV, Astron. Soc. Pac., San Francisco, p. 349
Krist J., Hook R., 2004, The Tiny Tim User's Guide, URL:www.stsci.edu/software/tynytim
Kroupa P., 2001, MNRAS, 322, 231
La Barbera F., Busarello G., Massarotti M., Merluzzi P., Capaccioli M., 2003, ApJ, 595, 127
Longhetti M., Saracco P., 2008, MNRAS, submitted
Longhetti M. et al., 2005, MNRAS, 361, 897
Longhetti M. et al., 2007, MNRAS, 374, 614
Maraston C., Daddi E., Renzini A., Cimatti A., Dickinson M., Papovich C., Pasquali A., Pirzkal N., 2006, ApJ, 652, 85
Marchesini D. et al., 2007, ApJ, 656, 42
McCarthy P. J. et al., 2001, ApJ, 560, L131
McCarthy P. J. et al., 2004, ApJ, 614, L9
McGrath E., Stockton A., Canalizo G., 2007, ApJ, 669, 241
McGrath E., Stockton A., Canalizo G., Iye M., Maihara T., 2008, ApJ, 682, 303
McIntosh D. H. et al., 2005, ApJ, 632, 191
Mei S. et al., 2006, ApJ, 644, 759
Moriondo G., Cimatti A., Daddi E., 2000, A&A, 364, 26
Naab T., Johansson P. H., Ostriker J. P., Efstathiou G., 2007, ApJ, 658, 710
Nipoti C., Londrillo P., Ciotti L., 2002, MNRAS, 332, 901
Peng C. Y., Ho L. C., Impey C. D., Rix H.-W., 2002, AJ, 124, 266
Pozzetti L. et al., 2003, A&A, 402, 837
Pozzetti L. et al., 2007, A&A, 474, 443
Renzini A., 2006, ARA&A, 44, 141
Rettura A. et al., 2008, ApJ, in press (arXiv:0806.4604)
Rix H.-W. et al., 2004, ApJS, 152, 163
Saracco P. et al., 2003, A&A, 398, 127
Saracco P. et al., 2005, MNRAS, 357, L40
Saracco P. et al., 2006, MNRAS, 367, 349
Sérsic J. L., 1968, Atlas de Galaxias Australes. Obs. Astron., Univ. Nac. Córdoba, Córdoba
Shen S. et al., 2003, MNRAS, 343, 978
Spinrad H., Dey A., Dunlop J., Peacock J., Jimenez R., Windhorst R., 1997, ApJ, 484, 601
Springel V., Hernquist L., 2005, ApJ, 622, L9
Stanford S. A. et al., 1997, AJ, 114, 2232
Stanford S. A. et al., 2004, ApJ, 127, 131
Tacconi L. J. et al., 2006, ApJ, 640, 228
Tacconi L. J., Genzel R., Smail I., 2008, ApJ, 680, 246
Treu T. et al., 2005, ApJ, 633, 174
Trujillo I. et al., 2004, ApJ, 604, 521
Trujillo I. et al., 2006a, MNRAS, 373, L36
Trujillo I. et al., 2006b, ApJ, 650, 18
Trujillo I., Conselice C. J., Bundy K., Cooper M. C., Eisenhardt P., Ellis R. S., 2007, MNRAS, 382, 109
van der Wel A., Holden B. P., Zirm A. W., Franx M., Rettura A., Illingworth G. D., Ford H. C., 2008, ApJ, 688, 48
van Dokkum P. G., 2005, AJ, 130, 2647
van Dokkum P. G., Stanford S. A., 2003, ApJ, 585, 78
van Dokkum P. G. et al., 2008, ApJ, 677, L5
Waddington I. et al., 2002, MNRAS, 336, 1342
Wolf C., Meisenheimer K., Rix H.-W., Borch A., Dye S., Kleinheinrich M., 2003, A&A, 401, 73
Zucca E. et al., 2006, A&A, 455, 879

APPENDIX A: PHOTOMETRY OF THE SAMPLE

In Table 1, the multiband photometry for the whole sample of ETGs is reported. With the exception of the F160W-band magnitude, which we have estimated on the *HST*-NICMOS images, the other magnitudes have been taken from the literature.

The photometry of the two galaxies in the HUDF previously studied by Daddi et al. (2005) and by Cimatti et al. (2008) comes from the catalogue of Coe et al. (2006). Namely, the *B*, *V*, *R*, *z* and *J* magnitudes are the magnitudes measured through the *HST* filters F435W, F606W, F775W, F850W and F110W, respectively. The *Ks*-band magnitude is taken from Cimatti et al. (2008) and comes from VLT-ISAAC observations in the *Ks* filter.

For the sample of Longhetti et al. (2005), the magnitudes are those from the MUNICS survey whose optical filters are slightly different from the standard Kron-Cousins filters. A detailed description of the MUNICS photometry and of the filter response is given by Drory et al. (2001).

The seven-filter (*B*, *V*, *R*, *I*, *z*, *H*, *K*) photometry of the 10 ETGs selected from the GDDS sample (Abraham et al. 2004) was originally taken from the photometric catalogues of the Las Campanas Infrared Survey (McCarthy et al. 2001). The observations of the fields, the filters used and the photometric information are described in Chen et al. (2002) and Firth et al. (2002).

The photometry of the six galaxies at $z \sim 1.27$ belonging to the cluster RDCS 0848+4453 in the Linx Supercluster is taken from Stanford et al. (1997). The three galaxies, CIG_135, CIG_108 and CIG_142, seem to coincide with the three galaxies studied by van Dokkum et al. (2003). The photometry is described in Stanford et al. (1997) and subsequent observations are quoted in Mei et al. (2006).

The photometry of the three galaxies in the HDF-N previously studied by Stanford et al. (2004) is partly taken from the HDF-N catalogue (v2). The magnitudes in the filters *B*, *V* and *I* are in fact the magnitudes measured through the *HST* filters F450W, F606W and F814W.

The photometry in the *R*, *H* and *K* bands of the galaxy 53W091 is taken from Dunlop et al. (1996) and Spinrad et al. (1997). The *I* and *J* magnitudes are the magnitudes in the F814W and F110W filters, respectively, taken from Waddington et al. (2002).

This paper has been typeset from a TEX/LATEX file prepared by the author.